

Article

# Estimating and Up-Scaling Fuel Moisture and Leaf Dry Matter Content of a Temperate Humid Forest Using Multi Resolution Remote Sensing Data

Hamed Adab <sup>1</sup>, Kasturi Devi Kanniah <sup>2,3,\*</sup> and Jason Beringer <sup>4</sup>

<sup>1</sup> Faculty of Geography and Environmental Science, Hakim Sabzevari University, Sabzevar, Khorasan Razavi 9617976487, Iran; h.adab@hsu.ac.ir

<sup>2</sup> Faculty of Geoinformation and Real Estate, Universiti Teknologi Malaysia, Johor 81310, Malaysia

<sup>3</sup> Centre for Environmental Sustainability and Water Security, Research Institute for Sustainable Environment, Universiti Teknologi Malaysia, Johor 81310, Malaysia

<sup>4</sup> School of Earth and Environment, University of Western Australia (M004), 35 Stirling Highway, Crawley WA 6009, Australia; jason.beringer@uwa.edu.au

\* Correspondence: kasturi@utm.my; Tel.: +60-7-553-0739

Academic Editors: Sangram Ganguly, Compton Tucker, Ioannis Gitas, Clement Atzberge and Prasad S. Thenkabail

Received: 27 June 2016; Accepted: 7 November 2016; Published: 19 November 2016

**Abstract:** Vegetation moisture and dry matter content are important indicators in predicting the behavior of fire and it is widely used in fire spread models. In this study, leaf fuel moisture content such as Live Fuel Moisture Content (LFMC), Leaf Relative Water Content (RWC), Dead Fuel Moisture Content (DFMC), and Leaf Dry Matter Content (LDMC) (hereinafter known as moisture content indices (MCI)) were calculated in the field for different forest species at 32 sites in a temperate humid forest (Zaringol forest) located in northeastern Iran. These data and several relevant vegetation-biophysical indices and atmospheric variables calculated using Landsat 7 Enhanced Thematic Mapper Plus (ETM+) data with moderate spatial resolution (30 m) were used to estimate MCI of the Zaringol forest using Artificial Neural Network (ANN) and Multiple Linear Regression (MLR) methods. The prediction of MCI using ANN showed that ETM+ predicted MCI slightly better (Mean Absolute Percentage Error (MAPE) of 6%–12%) than MLR (MAPE between 8% and 17%). Once satisfactory results in estimating MCI were obtained by using ANN from ETM+ data, these data were then upscaled to estimate MCI using MODIS data for daily monitoring of leaf water and leaf dry matter content at 500 m spatial resolution. For MODIS derived LFMC, LDMC, RWC, and DLMC, the ANN produced a MAPE between 11% and 29% for the indices compared to MLR which produced an MAPE of 14%–33%. In conclusion, we suggest that upscaling is necessary for solving the scale discrepancy problems between the indicators and low spatial resolution MODIS data. The scaling up of MCI could be used for pre-fire alert system and thereby can detect fire prone areas in near real time for fire-fighting operations.

**Keywords:** leaf moisture content; leaf dry matter content; temperate humid forest; remote sensing; artificial neural network; multiple linear regression; upscaling; fire danger

## 1. Introduction

Fire is a common form of disaster in forested and grassland areas across temperate regions of the world. Although fire is a critical environmental issue in many regions, including Iran, there is no adequate monitoring or detection of fire in Iran and that makes fire detection and control quite difficult. Intervention of forest fires can occur at an early stage of fire ignition by monitoring and forecasting the factors such as leaf moisture content and leaf dry matter content (MCI) that influence biomass burning.

A comprehensive collection of relevant environmental variables is required to understand fire occurrence and hazard. Fuel moisture content is an important parameter in the heat energy of pre-ignition because fuel moisture content restricts water vapor released from burning fuel in the preheating phase [1]. Indices of vegetation moisture have a relationship with the fire probability because when plants experience water deficits or nutrients stress, leaves may eventually become more yellow and brown so the vegetation indices will then change. Decreasing vegetation indices suggest an increased fire probability where stressed plants are more vulnerable to fire ignition [2]. Fuel moisture content influences fire behavior (slow or fast spread), propagation, intensity, ignition delay, the degree of flammability and the emissive power of flames. The relationship between ignitability and leaf dry matter will help us to understand the functional role (fuel load) of leaf in fire-prone ecosystems as leaves with low dry matter will have reduced ignitability [3]. Hence, fuel moisture and plant dry matter are considered to be important parameters in any forest fire modeling that attempts to predict fuel ignition. Such models can be used to provide early warning of increased forest fire potential at the pre-ignition stage.

There are a number of fire early warning systems based on remote sensing and Geographic Information System such as the Canadian Forest Fire Danger Rating System (CFFDRS) [4], Forest Fire Danger Forecasting System (FFDFS) [5], and early warning system for wildfire (EWSFire) [6] that all have varying structural and/or dynamic parameters (e.g., slope, aspect, elevation, and weather variables). However, there is inadequate availability of information on live and dead fuel moisture contents in Iran that makes forest fire hard to predict. Commonly used indicators for moisture content are Live Fuel Moisture Content (LFMC), Leaf Relative Water Content (RWC), Dead Fuel Moisture Content (DFMC), whilst Leaf Dry Matter Content (LDMC) is an important plant functional trait in plant studies because it is related to many critical aspects of a plant's performance in response to environmental changes during plants' growth and survival [7]. These indicators are very important for monitoring forest fire that may change under different heat and water stress conditions such as drought and severe heat wave.

Among the fuel moisture indices, LFMC has been widely used for fire danger studies [8,9] because it is not only simple to calculate but also the ignition delay and degree of flammability (the quantity of heat necessary to evaporate water) are correlated to the amount of water in live fuels [1]. In areas of high vegetation productivity, such as this study, a small reduction in fuel moisture may enhance the dry matter productivity (i.e., an increase in dead fuel load and connectivity) [10], and therefore fuel consumption is increased by fire. LDMC is related to the lifecycle of a leaf and it shows the production of dry matter per leaf [11] and is a plant trait that sets the amount of dry material that is available for combustion [12]. Flammability of fuel is expected to be greater in tree species with high leaf dry matter content [12] and increases as a function of the drying rate of live or dead material. DFMC is a significant parameter in most empirical models for fire spread [13]. Variation of fine dead fuel moisture such as needles, leaves, twigs, and bark can be influenced by air temperature, relative humidity, moisture content of duff, and topsoil. RWC has been widely accepted as a meaningful index of plant water status and water balance of a plant because leaf photosynthetic activity decreases as RWC is reduced under plant water stress [11]. RWC could be a useful parameter as it has previously been used to screen for drought tolerance of tree species [14]. Thus, LFMC and DFMC are broadly used in early warning fire systems but RWC and LDMC could be also assessed as alternatives to implement them in early warning systems.

One of the methods used to measure moisture content and dry matter content in the field is the gravimetric method for specific classes of fuels, such as live and dead. This method is easy to use, involves high levels of accuracy, and can be performed on different fuel types (e.g., leaves and branches), however, it is time consuming, often requires destructive sampling, is labor intensive and is costly to conduct repetitive samplings over large areas. Additionally, these measurements are point based and do not have uniform and extensive spatial coverage of the study area. Alternatively, remote sensing data provides an instantaneous and non-destructive way for vegetation studies at large

scales because it presents a quick look evaluation of the vegetation conditions, which is important for water stress detection and fire hazard assessment. Changes in the water content of vegetation can result in different spectral characteristics that provide the potential to estimate the status of vegetation moisture using spectral data [15]. According to the electromagnetic spectrum, there is a link between a plant's moisture content and its spectrum. The spectral responses for live fuel moisture levels were explored in the visible, NIR (near-infrared), SWIR (short-wave infrared) and thermal infrared wavelengths, so these wavelengths are used to estimate fuel moisture content [16]. On the other hand, dead fuel moisture is primarily affected by soil moisture (which would also be affected by weather) near the dead fuel surface [17]. Some studies showed that surface soil moisture could be estimated using optical data for croplands, short grass lands [18,19], and forest-dominated areas (deciduous species) [20]. Given this information, vegetation indices could be used indirectly to estimate dead leaves covering the forest floor.

A great deal of effort has gone into estimating DFMC and LFMC using meteorological variables and remote sensing data (See Table 1 for more details). Previous studies have estimated LFMC using coarse spatial resolution remote sensing data such as MODerate resolution Imaging Spectroradiometer (MODIS) and Advanced Very High Resolution Radiometer (AVHRR) usually by making a direct comparison between field measurements and large view angle remote-sensing data [21,22]. This can be done if the surface is large and perfectly homogeneous or a sufficient number of point measurements can be made during the satellite overpass [23]. MODIS and AVHRR have high temporal resolution which makes them useful for providing fuel moisture content in near real time because moisture content of the fuel is a function of short term vegetation-biophysical indices and atmospheric variables. Nevertheless, the estimation of accurate leaf water-content and dry matter information is currently critically limited because of the disparity in scale between ground measurements (plot based) and lower spatial resolution remote sensing data (i.e., 1 km). Such coarser resolution information does not give enough detail for some fire management activities and, therefore, satellite data with high to moderate spatial resolution is desired for upscaling ground measured MCI before low spatial resolution data can be used to provide estimates of MCI over a regional scale in near real-time. Hence, upscaling ground "point" measurements from ETM to the MODIS resolutions using high-resolution remotely sensed imagery is a necessary and critical step to obtain accurate MCI from MODIS data. Thus, the aim of this study was to quantify MCI (leaf water-related properties LFMC, DFMC, RWC and dry matter content (LDMC)) using daily field measurements in a temperate humid forest in Iran and then to spatially predict MCI using remotely sensed data with Landsat Enhanced Thematic Mapper plus (ETM+). Daily maps of MCI are derived by upscaling MCI from plot scale to higher spatial resolution satellite data (30 m) and from higher spatial to higher temporal resolution (daily) satellite images (MODIS) at 500 m spatial resolution. The data and methods adopted to achieve the aim of the study are described in the following sections.

**Table 1.** Overview of models/statistical methods used to estimating live and dead fuel moisture content using meteorological and remote sensing data.

Type of Fuel	Parameters Used	Satellite Data	Vegetation Type (Study Area)	Method	Reference
Litter Dead fuel	Relative Humidity (RH), Air Temperature (AT), Wind Speed, Cloudiness	Not used	Red Pine forests-Taiwan	Linear Regression (LR) R = 0.7	[24]
Litter Dead fuel	AT, RH, Precipitation, Incoming Solar Radiation; Moisture Content, Fuel Surface Temperature, wind speed and direction	Not used	Grasses and herbaceous vegetation-Hawaii	LR R = 0.01–0.85	[25]
Litter, Grasslands Dead fuel	Temperature, Humidity	Not used	Grasslands, shrubs and deciduous-Spain	LR R = 0.11–0.52	[26]

Table 1. Cont.

Type of Fuel	Parameters Used	Satellite Data	Vegetation Type (Study Area)	Method	Reference
Litter Dead fuel	Maximum Daily Temperature, Minimum Daily RH	Not used	Jarrah and Karri forests-southwest Western Australia	LR R = 0.66	[27]
Live leaves	NDVI, LST, Relative Greenness Index (RGRE)	AVHRR	Herbaceous and shrubs-Spain	LR R = 0.68	[22]
Live leaves	MSI, NDWI, Water Index (WI), TM5/TM7, Global Vegetation Moisture Index (GVMI)	LOPEX	Mediterranean Species-UK	LR R = 0.71	[28]
Live leaves	NDVI, NDWI	MODIS	Shrubs-US	LR R = 0.6–0.8	[29]
Live leaves	NDVI, NDWI, Vegetation Dryness Index (VDI), Improved VDI (IVDI), Accumulated Relative NDVI Decrement (ARND)	SPOT veg	Herbaceous-South Africa	LR R = 0.75	[30]
Live leaves	NDWI, Normalized Difference Infrared Index (NDII)	MODIS	Cypress stands, shrubs-US	LR R = 0.51	[31]
Live leaves	NDII, NDWI, Visible Atmospheric Resistant Index (VARI)	MODIS	Chaparral (shrubs)-US	LR R = 0.72	[32]
Live leaves	Shortwave Infrared Water Stress Index (SIWSI)	MODIS	Tropical rainforests-Malaysia	LR R = 0.68	[33]
Live leaves	NDVI, Soil Adjusted Vegetation Index (SAVI), Enhanced Vegetation Index (EVI), Global Environmental Monitoring Index (GEMI), VARI, NDII, NDWI, Global Vegetation Moisture Index (GVMI)	MODIS	Grasslands and shrub-lands-Spain	IM, LR R = 0.7–0.92	[34]
Live leaves	VARI, NDVI	MODIS	Evergreen shrub, brush-US	LR R = 0.72	[21]
Live leaves	NDVI, NDWI, NDII, Vegetation Index (VI green), VARI, Enhanced Vegetation Index (EVI)	MODIS	Chaparral, coastal sage scrub-US	LR R = 0.72–0.85	[35]
Live leaves	NDVI, VARI, NDWI, NDII, MSI, SRWI, Spectral Reflectance	MODIS	Deciduous forest-Argentina	LR R = 0.72	[36]
Live leaves	NDVI, NDWI, Canopy Water Content (CWC), Soil moisture (SM)	MODIS	Gambel oak and big sagebrush-US	LR R = 0.49	[37]
Live leaves	NDWI, NDII, SRWI, MSI, GVMI	MODIS	Savanna-Senegal	LR R = 0.63	[38]
Live leaves	Spectral Reflectance range 410–2500 nm	LOPEX	Area of the JRC, Ispra, Italy	GA-PLS regression R <sup>2</sup> = 0.87–0.89	[39]
Live leaves	Spectral Reflectance range 400–2500 nm	LOPEX	Area of the JRC, Ispra, Italy	PLS R <sup>2</sup> = 0.74–0.92	[40]

LR = Information not available.

## 2. Materials and Methods

### 2.1. Study Area

Northern Iran is an understudied area in terms of forest fire monitoring and management which requires appropriate attention. The region contains the Northeastern Hyrcanian forests (Golestan province) that are one of the most critical areas in terms of forest fire in Iran where, for example, in November 2010 more than 80 fires occurred in this area and 70 protected areas of the forests were affected by fires [41]. Fires are mainly in the form of surface fires and the extremely dry conditions in the forested area in this year were the major cause of widespread fires [41]. It seems that these forests experience fires every year and the number of fire incidents increased from 2001 to 2008. Most land fires occur in this region during the time when the leaves are still green (August until the end of December) due to a decrease in humidity and increase in wind speed [42]. It has been shown

in the study area that elevation is inversely correlated with fire hazard (94%) because of its influence on rainfall, temperature, fuel moisture content and population density [43].

One possible way to reduce the impact of fires on the forest ecosystem is by mapping the MCI of the forest and thereby providing early warning of forest fire at the pre-ignition stage. We utilized the Zaringol forest within the vulnerable Hyrcanian forests to test and evaluate our approach. The Hyrcanian forests are found along the coast of the Caspian Sea of Iran and are important refugia, as they comprise the last remnants of temperate deciduous broadleaved forests in this part of the world. Hyrcanian forests consist of mixed broadleaf deciduous species. These natural mixed-hardwood forests have rich tree species diversity such as beech (*Fagus orientalis*), hornbeam (*Carpinus betulus*), alder (*Alnus glutinosa*), oak (*Quercus castaneifolia*), maple (*Acer velotonia*), ironwood (*Parrotia persica*), etc. [44]. The Zaringol forest is one of the Hyrcanian forests found in the province of Golestan and these forests are found on a hillside about 15 km southeast of the city of Aliabad-e Katul (Figure 1a) and 50 km east of the city of Gorgan. As shown in Figure 1b, eight dominant forest species, namely *Crataegus* sp., *Parrotia persica*, *Acer* sp., *Quercus castaneifolia*, *Alnus subcordata*, *Pinus* sp., *Carpinus schuschaensis*, and *Carpinus betulus*, are found in the Zaringol forest area.

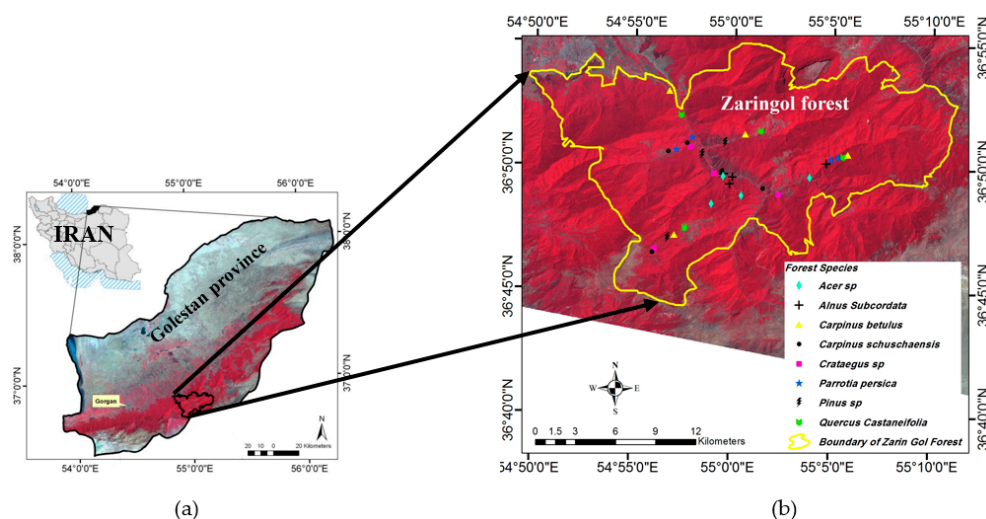


**Figure 1.** (a) Location of the province of Golestan in Iran; (b) boundary of Zaringol forest in Golestan province and location of the 32 sampling sites that cover different forest species in the Zaringol forest area. Locations are shown on ETM+ satellite image dated 20 July 2000.

## 2.2. In Situ Leaf Moisture and Dry Matter Content Data Collection

In this study, we collected live (including shedding and non-shedding leaves as possible) and also dead leaves from tree branches and the forest floor in the field in Southeast Aliabad region (Figure 1). Leaves were collected from 32 sampling plots where each sampling plot had an area of  $30 \times 30 \text{ m}^2$ . This size was used for sampling because each Landsat ETM+ pixel represents a  $30 \times 30 \text{ m}^2$  ground area and samples were collected within  $5 \times 5 \text{ m}^2$  and  $15 \times 15 \text{ m}^2$  from the center of the plot at four cardinal directions (north, east, south, and west). Live and dead leaves were collected from 8 trees from each sampling plot per species (i.e., the samples of live and dead leaves were not mixed together) at different locations covering different elevation, slope gradient, and aspect over a period of 3 days (5–7 August 2012) with the help of forest experts from the Golestan Forests, Range and Watershed Management Organization. Dead and live leaf samples were collected when no rainfall occurred in the previous week to avoid the effect of surface water on the leaves, especially for dead leaves. Most samples were collected in locations with slopes of less than  $22^\circ$  because steep slopes are not easily accessible. Four full zip locked bags of live and dead leaves were collected (60 g each) between 11:00 a.m. and 16:00 p.m. local time, as this period coincides with the Landsat overpass time in the

study area and, when the air temperature was at its highest, most stable and when fuel was most vulnerable to ignitions [45]. All live samples were immediately measured for their fresh weight using an electronic balance with 0.01 g precision. These samples were further processed in the laboratory to measure their moisture content. All the live leaves were placed in a bucket of cold distilled water and were stored in a refrigerator for 24 h to determine their turgid weight (weight obtained after rehydrating leaves to full water saturation). The temperature of the refrigerator was set to 4 °C and a fan was used to homogenize cool air inside the refrigerator. Then, the live leaves were removed from the refrigerator to find the weight of turgid leaves using the turgid measurement protocol [46]. Any water remaining on the leaves were removed using tissue paper and the weights of the turgid leaves were measured. The samples were then transferred to an oven for drying where they remained at 70 °C for 48 h. All collected dead samples were also oven-dried for 24 h at a temperature of 100 °C [47]. The samples (both live and dead leaves) were then weighed again using an electronic balance.

### 2.3. Calculation of Leaf Moisture and Dry Matter Content

The four MCI calculated in this study and the equations used to calculate them are shown in Table 2. A one way analysis of variance (ANOVA) and coefficient of determination ( $R^2$ ) were computed to describe the relationships between MCIs and different species. ANOVA tests the hypothesis that the mean values of different MCIs of eight different forest tree species are equal.

**Table 2.** Leaf moisture and dry matter content indices (MCI) calculated in this study.

MCI	Calculated Equation
Live Fuel Moisture Content (LFMC)	$LFMC = \frac{M_f - M_d}{M_d} \times 100 (\%)$
Dead Fuel Moisture Content (DFMC)	$DFMC = \frac{M_{fm} - M_d}{M_d} \times 100 (\%)$
Leaf Dry Matter Content (LDMC)	$LDMC = \frac{M_d}{M_t} \times 100 (\%)$
Leaf Relative Water Content (RWC)	$RWC = \frac{M_f - M_d}{M_t - M_d} \times 100 (\%)$

Notes:  $M_f$  is the fresh weight of live leaves that were measured in the field during sampling,  $M_d$  is the weight of the same sample of leaves after they were oven-dried.  $M_t$  is the turgid mass after rehydrating the leaves, and  $M_{fm}$  is the fresh weight of dead materials that was measured in the field [48].

### 2.4. Remotely Sensed Data

Landsat 7 ETM+ and MODIS data were used to calculate vegetation and biophysical indices, and retrieve atmospheric variables to estimate the four MCI as shown in Table 2. This study used one scene of level 1T Landsat 7 ETM+ SLC-off image dated 6 August 2012 acquired at 11:20 a.m. local time (coinciding with field measurements) provided by the USGS Global Visualization server (GloVis) at <http://glovis.usgs.gov/> in GeoTIFF file format. In addition, MODIS level 1B (calibrated and geo-located radiance product) data on board the Terra satellite with 500 m (MOD02HKM) and 1 km (MOD021KM) spatial resolution and their geolocation products with 1 km (MOD03) were downloaded with the same overpass time as the ETM+ image. On 6 August 2012, MODIS crosses the study area at 11:40 a.m. local time (Terra) and 1:20 p.m. local time (Aqua) during the daytime dated 6 August 2012, thus vegetation and temperature conditions can be retrieved twice daily. Although we only demonstrate the utility of this approach with a single image, the high temporal frequency is critical for operational monitoring of fuel moisture content and providing an early warning of forest fire potential.

### 2.5. Pre-Processing of Remote Sensing Data

The ETM+ image was atmospherically and topographically corrected using the ATCOR3 program that is used for mountainous areas <3.5 km above sea level. The thermal bands of this image were corrected for atmospheric attenuation using the Radiative Transfer Equation Atmospheric

Correction Parameters Calculator (RTE-ACPC), an online web-based tool that was developed by Barsi, et al. [49]. For MODIS data, the SMAC (Simplified Method for Atmospheric Correction) program was used for atmospheric correction of the first 7 bands, whilst the thermal bands of MODIS data (Bands 31 and 32) were corrected using a split-window algorithm [50] which was used to retrieve land surface temperature. This method can correct the thermal bands using water vapor content and surface emissivity data [51].

The MODIS image was geometrically corrected by selecting control points (CPs) from ETM+ image dated 10 May 2003 had been geometrically corrected by the National Cartographic Center of Iran (NCC). CPs were selected from well-defined locations such as road junctions, intersections, and other well defined features. The total RMS location errors of the ETM+ and MODIS images were 0.52 and 0.54 pixels, respectively. The Landsat 7 ETM+ sensor had a Scan Line Corrector (SLC) failure where all Landsat ETM+ images have a wedge-shaped gap on both sides of a scene, resulting in approximately 22% data loss [52]. We tested several gap filling methods including USGS gap fill method (triangulation interpolation), Inverse Distance Weight, Local Polynomial Interpolation (LPI), Radial Basis Functions, and Kriging with different variogram models and compared them with the simulated SLC-off images, which helped us to understand their accuracy quantitatively. The result showed that Kriging could accurately describe the spatial dependence of gaps (an overall RMSE value of 5 raw DN value). Geostatistical methods (kriging or co-kriging) are commonly used as the most suitable method to fill the data gaps [53,54]. Thus, we used the kriging interpolation technique as the most suitable method for estimating pixel values (DN) for locations that had gaps (no data) in ETM+ raw data [53,54] (dated 6 August 2012) covering the Zaringol area for all bands except for the panchromatic band (band 8). There were repetitive stripes over the entire image of MODIS Terra band 5 (1.230–1.250  $\mu\text{m}$ ). Band 5 was used in this study to calculate the vegetation and bio-physical indices such as Albedo and the Normal Difference Water Index (NDWI) as a measure of fuel moisture content. Similar to the processing of Landsat ETM+, kriging (ordinary) interpolation was used to correct the stripe noise of Band 5 of the MODIS data (dated 6 August 2012). Various vegetation indices, biophysical and atmospheric variables that are relevant to estimating MCI in this study are provided in Appendix A.

### 2.6. Upscaling In Situ Leaf Moisture and Leaf Dry Matter Content Using Landsat ETM+ Data

Upscaling is a way of taking information based on observations that have a small spatial domain and extending that domain to a larger geographic area. MCI calculated using field data were combined with spectral indices calculated using ETM+ data to develop empirical models to estimate MCI at a large spatial scale. Both Multiple Linear Regressions (MLR) and Artificial Neural Network (ANN) techniques were used for scaling up (see below). We identified 13 parameters (vegetation indices, biophysical and atmospheric variables) that were potentially relevant to the estimation of MCI (Appendix A) along with the subset of specific ones used in this study. As our predictor variables include multiple factors, multicollinearity can be a computational problem that arises in the analysis of regression and ANN models when there is inter-correlation between several independent variables. As a result of the interrelationships, Principle Component Analysis (PCA) was used in this study to reduce the collinearity of the predictor variables, which can extract the smaller number of uncorrelated components for modeling. We reduced the initial set of 13 parameters to 4 pertinent ones by utilizing a PCA. The first and second principal components usually contain the most variance. However, in order to extract the greatest information from these predictor variables the Varimax rotation (a procedure in which the eigenvectors/factors are rotated in an attempt to achieve simple structure) of PCA was used.

Varimax1 and Varimax2 were used to generate two different sets of equations for ETM+; one for DFMC and another one for LFMC, RWC, and LDMC as shown in Equations (1)–(4). The PCA consists of a transformation of the input dataset (e.g., Air temperature, RH, LST, LAI and Albedo for Equation (1)) to reduce the dimensionality of data sets and produce uncorrelated output data. The first and second

Varimaxes were extracted from Equations (1) and (4) which explain the total variance of 80% for Equations (1) and (2) and 84% for Equations (3) and (4).

$$\text{VARIMAX}_{1\text{DFMC}} = (0.13 \times \text{AIRTEMPERATURE}) + (0.017 \times \text{RH}) + (0.11 \times \text{LST}) + (-0.34 \times \text{LAI}) + (0.08 \times \text{ALBEDO}) + (-10.34) \quad (1)$$

$$\text{VARIMAX}_{2\text{DFMC}} = (-0.084 \times \text{AIRTEMPERATURE}) + (0.094 \times \text{RH}) + (0.02 \times \text{LST}) + (0.28 \times \text{LAI}) + (0.08 \times \text{ALBEDO}) + (-6.07) \quad (2)$$

$$\begin{aligned} \text{VARIMAX}_{1\text{LFMC,RWC, and LDMC}} &= (1.02 \times \text{GBNDVI}) + (0.0002 \times \text{NCI}) + (2.04 \times \text{NDII}) + (0.58 \times \text{NDVI}) \\ &+ (2.99 \times \text{NDWI}) + (0.61 \times \text{OSAVI}) + (0.53 \times \text{SLAVI}) + (0.61 \times \text{VARINIR}) \\ &+ (0.07 \times \text{AIRTEMPERATURE}) + (0.03 \times \text{RH}) + (0.05 \times \text{LST}) + (0.1 \\ &\times \text{LAI}) + (0.05 \times \text{ALBEDO}) + (-12.47) \end{aligned} \quad (3)$$

$$\begin{aligned} \text{VARIMAX}_{2\text{LFMC,RWC, and LDMC}} &= (-0.68 \times \text{GBNDVI}) + (-1.75 \times \text{NCI}) + (0.97 \times \text{NDII}) \\ &+ (-0.89 \times \text{NDVI}) + (1.59 \times \text{NDWI}) + (-0.86 \times \text{OSAVI}) \\ &+ (0.23 \times \text{SLAVI}) + (-0.86 \times \text{VARINIR}) \\ &+ (0.13 \times \text{AIRTEMPERATURE}) + (0.03 \times \text{RH}) + (0.1 \times \text{LST}) \\ &+ (-0.09 \times \text{LAI}) + (0.07 \times \text{ALBEDO}) + (-8.52) \end{aligned} \quad (4)$$

### 2.6.1. Multiple Linear Regression (MLR)

Multiple linear regression (MLR) is a form of linear regression that is used to model the relationship between two or more independent variables and a dependent variable by finding the best-fitting linear equation to observed data. MLR analysis was conducted to estimate MCI over the entire study area of Zaringol. Varimax1 and Varimax2 (Equations (1)–(4)) were used instead of the 13 and 5 variables as shown in MLR Equations (5)–(8). Out of a total of 32 samples, 77% of the data collected in the field were used to train the MLR model in the regression analysis, while the remaining 23% were used for validating the performance of the model.

$$\text{RWC} = 64.4 + 7.6X_1 + (-8.83X_2) \quad (5)$$

$$\text{LDMC} = 25.15 + (-2.85X_1) + 3.61X_2 \quad (6)$$

$$\text{LFMC} = 183.44 + 51.29X_1 + (-34.35X_2) \quad (7)$$

$$\text{DFMC} = 17 + (-3.26X_1) + 4.1X_2 \quad (8)$$

where  $X_1$  and  $X_2$  are Varimax1 and Varimax2, respectively.

### 2.6.2. Artificial Neural Network (ANN)

Typically, neural networks are organized in layers. In this study, the typology of the ANN used to estimate MCI from ETM+ data consisted of an input layer, a hidden layer, and an output layer. In the input layer, the neurons perform preprocessing procedures on input data (e.g., Varimax1 and Varimax2) such as normalization or scaling. However, the main processing occurs in the hidden and output layers. There are neurons in the hidden layer and output layer. Each neuron has an activation function that connects the output of a neuron to a given input. One hidden layer is usually enough in such networks to realize any relating input to output data [55]. The size of the hidden neurons is between the size of input and output layers. Based on [56], three neurons in one hidden layer of a network structure were used in this study for the two input layers (Varimax1 and Varimax2 obtained from PCA (Equations (1)–(4)) and one output layer, either LFMC, RWC, LDMC, or DFMC. The activation function of the hidden layers used in this study was Tanh Axon which applies a bias and tanh function

to each neuron in the layer. The algorithm used for training is the feed forward multilayer perceptron (MLP) using the Levenberg Marquardt back-propagation method. The Newton Levenberg Marquardt was used for training the ANN because it does not need learning rates and momentum making them easier to use compared to the backpropagation method [57]. The data set was divided into training, testing, and validation. Out of a total of 32 samples, 65% (21 plots) of the data set was used for training, 23% (7 plots) was used for cross validation, and 12% (4 plots) was used for random testing. During training the ANN, mean squared error (MSE) was used to keep the network from overfitting.

### 2.7. Upscaling Fuel Moisture and Leaf Dry Matter Content Derived from ETM+ to MODIS

Although Landsat ETM+ can provide comparatively detailed information on MCI at a large spatial extent, these data are not suitable for daily monitoring of MCI, which is critical for forest fire monitoring. Therefore, we used MODIS data that has daily coverage over the study area. We up-scaled MCI estimated using ETM+ data to MODIS data resolution using MLR and ANN techniques. The MCI estimated from Landsat ETM+ were aggregated from 30 m to 500 m using the nearest neighbor resampling method, a common up-scaling scheme. The structural similarity index (SSI) was used to compare the original 30 m MCI and aggregated 500 m MCI. SSI was used mainly to measure the structural information similarities between the two images, which is better than traditional methods such as peak signal-to-noise ratio (PSNR) and mean squared error (MSE).

The same vegetation indices and biophysical and atmospheric variables (Appendix A) were calculated using MODIS data and these parameters were correlated with resampled MCI at 500 m. Direct upscaling from in-situ MCI measurements (30 m) to MODIS data (500 m) may cause errors when estimating MCI because of the scale discrepancy between these data sets as explained in Section 3.3. As for the ETM+ data, we used PCA to retrieve fewer and less co-related spectral indices and atmospheric variables calculated using MODIS data. The Pearson correlation was used to determine the maximum possible relationship of each factor to four MCI indicators. A high correlation was found between both Varimax1 and Varimax2 with LFMC ( $R = 0.8$  and  $0.03$ ), RWC ( $R = 0.84$  and  $-0.1$ ) and LDMC ( $R = -0.84$  and  $-0.07$ ). For DFMC the first two components of PCA produced higher correlation coefficient ( $R = -0.6$  and  $0.52$ ) compared to Varimax1 and Varimax2 ( $-0.58$  and  $0.23$ ) therefore, Principle components 1 and 2 were used to estimate DFMC. The aggregated ETM+ MCI at 500 m and Varimax1 and Varimax2 were used to estimate LFMC, RWC, and LDMC and PC 1 and 2 of PCA were used to estimate DFMC. Two different sets of equations were generated, one for DFMC and another one for LFMC, RWC, and LDMC as shown in Equations (9)–(12). The first and second principal components in Equations (9) and (10) explained 83% and 90% of the total variation in Equations (11) and (12), respectively.

$$\begin{aligned} \text{Principle Component}_{1\text{DFMC}} &= (0.13 \times \text{LST}) + (0.2 \times \text{AIRTEMPERATURE}) + (20.28 \\ &\times \text{ALBEDO}) + (-0.87 \times \text{LAI}) + (0.04 \times \text{RH}) + (-12.55) \end{aligned} \quad (9)$$

$$\begin{aligned} \text{Principle Component}_{2\text{DFMC}} &= (-0.03 \times \text{LST}) + (-0.03 \times \text{AIRTEMPERATURE}) + (0.36 \\ &\times \text{ALBEDO}) + (0.76 \times \text{LAI}) + (0.12 \times \text{RH}) + (-3.46) \end{aligned} \quad (10)$$

$$\begin{aligned} \text{VARIMAX}_{1\text{LFMC,RWC,and LDMC}} &= (0.0017 \times \text{LST}) + (0.0076 \times \text{AIRTEMPERATURE}) \\ &+ (6.3 \times \text{ALBEDO}) + (0.83 \times \text{GBNDVI}) + (1.79 \times \text{NDWI}) + (0.95 \\ &\times \text{VARINIR}) + (0.22 \times \text{SLAVI}) + (0.23 \times \text{LAI}) + (0.03 \times \text{RH}) \\ &+ (1.56 \times \text{OSAVI}) + (0.89 \times \text{NDVI}) + (0.95 \times \text{NDII}) + (0.7 \times \text{NCI}) \\ &+ (-6.17) \end{aligned} \quad (11)$$

$$\begin{aligned}
& \text{VARIMAX}_{2\text{LFMC,RWC, and LDMC}} \\
& = (0.05 \times \text{LST}) + (0.099 \times \text{AIRTEMPERATURE}) \\
& + (21.2 \times \text{ALBEDO}) + (0.17 \times \text{GBNDVI}) + (1.52 \times \text{NDWI}) + (0.39 \\
& \times \text{VARINIR}) + (0.12 \times \text{SLAVI}) + (0.09 \times \text{LAI}) (0.08 \times \text{RH}) \\
& + (1.13 \times \text{OSAVI}) + (0.33 \times \text{NDVI}) + (0.61 \times \text{NDII}) + (-2.3 \times \text{NCI}) \\
& + (-11.37)
\end{aligned} \tag{12}$$

### 2.7.1. Multiple Linear Regression (MLR)

Principle components 1 (PC1) and 2 (PC2) and Varimax1 and Varimax2 (Equations (9)–(12)) were used to estimate LFMC, RWC, LDMC, and DFMC using MLR as shown in Equations (13)–(16). Approximately 77% of the study area (2029 pixels) was used to train the model, and 15% (606 pixels) was used to validate the performance of the model.

$$\text{RWC} = 69.57 + 11.16X_1 + (-6.71X_2) \tag{13}$$

$$\text{LDMC} = 2497 + (-8.18X_1) + 2.74X_2 \tag{14}$$

$$\text{LFMC} = 209.81 + 61.84X_1 + (-23.32X_2) \tag{15}$$

$$\text{DFMC} = 18 + (-1.39X_1) + 2.60X_2 \tag{16}$$

where  $X_1$  and  $X_2$  indicate VARIMAX1, VARIMAX2 (for LFMC, RWC, LDMC), and PC1, and PC2 (for DFMC).

### 2.7.2. Artificial Neural Network (ANN)

The structure of the ANN model implemented to estimate MCI from MODIS was similar to the structure implemented with the ETM+ data. However, the input layers were Varimax1, Varimax2, PC1 and PC2 which were obtained from PCA (Equations (9)–(12)). Approximately 65% (1713 pixels) of the aggregated MCI dataset were used to train the ANN, 23% (606 pixels) was used for cross validation, and the remaining 12% (316 pixels) was used to assess the accuracy of the results produced by ANN and also for the optimization of the ANN model. In this study, cross validation was used to detect over-fitting of data during the training stage of the neural network. This analysis stops training to avoid over-fitting in the output (LFMC, RWC, LDMC, and DFMC) and the performance of the model can be accurately assessed and Mean Square Error (MSE) was used to avoid ANN over fitting (ANN was stopped when the MSE began to rise).

### 2.8. Validation of Empirical Models

The results of estimated MCI indicators (using ANN and MLR models) using Landsat ETM+ (30 m) were validated with MCI data collected in the field (30 m plot size). Subsequently, the results of MCI estimated using MODIS data were validated with MCI estimated by ETM+ (aggregated pixels from 30 m to 500 m to match with the MODIS data). Various statistical measures such as Root Mean Square Error (RMSE), Mean Absolute Error (MAE) and the Mean Absolute Percentage Error (MAPE) were used to validate results from the model. The aggregated Landsat products and the MODIS products were compared using the residual standard error measure which shows the difference (residuals) between values of MODIS derived indices (LFMC, RWC, LDMC, and DFMC values) and aggregated MCI metrics from ETM+. This is a useful method because it represents the spatial differences of aggregated Landsat MCI and MODIS MCI between ANN and MLR. It can clearly show locations with similar or dissimilar MCI values obtained from both MLR and ANN techniques. A value of zero residual standard error means MODIS derived indices (either using ANN or MLR) were similar to the MCI metrics aggregated from ETM+ data.

### 3. Results

#### 3.1. Leaf Moisture and Dry Matter Content (MCI)

MCI calculated using data collected in the field are shown in Figure 2 and show that most of the species have a large range of values except for *Ainus Subcordata*, however, there was no inter-species variation between all the four MCI metrics. The  $R^2$  values suggest that 38%, 35%, 33%, and 26% of the variability in LFMC, RWC, LDMC, and DFMC was explained by different species (data not shown). Results of the analysis of variance (ANOVA) also indicated that the influence of species on MCI indicators was not statistically significant ( $p$  values  $> 0.05$ ). The results of ANOVA are as follows:

$$\text{LFMC}-(F_8, 32 = 2.09, p = 0.08)$$

$$\text{RWC}-(F_8, 32 = 1.81, p = 0.13)$$

$$\text{LDMC}-(F_8, 32 = 1.70, p = 0.15)$$

$$\text{DFMC}-(F_8, 32 = 1.20, p = 0.34)$$

where  $F_8, 32$  = number of tree species considered in this study from a total of 32 samples collected in the field.  $p$  = significance level (any  $p$  values of more than 0.05 shows the difference in MCI values among the 8 tree species is not statistically significant at 95% confidence level).

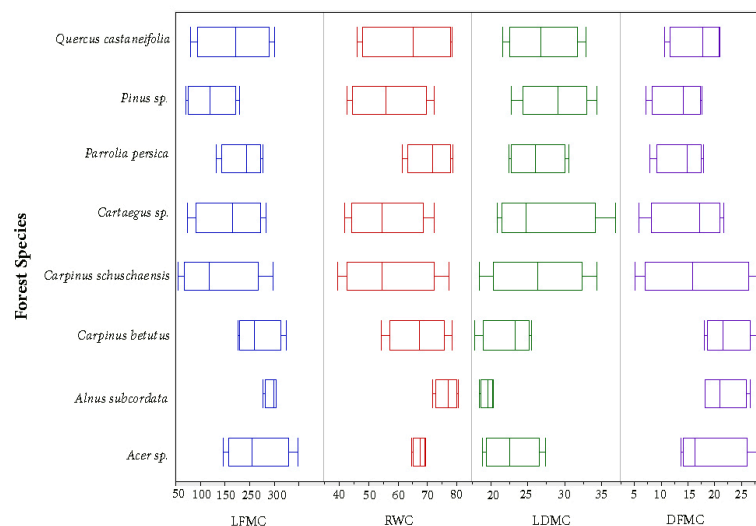


**Figure 2.** Box plots showing the distribution of MCI calculated using data collected in the field. Whiskers represent highest and lowest value of MCI metrics, solid lines of the box represent the median and the 25th and 75th percentiles.

#### 3.2. Validation of Leaf Moisture and Dry Matter Content (MCI) Estimations Using Satellite Data

MCI estimated using satellite data were validated using MCI that was determined using field data (Figure 2). The validation results using MAPE (Table 3) showed that the error of estimation of LFMC (5.9%), LDMC (7.7%), and DFMC (12.2%) from ETM+ for ANN was lower compared to LFMC (16%), LDMC (17.3%), and DFMC (16.6%) for MLR. In addition, the RMSE and MAE values derived from the ANN model for these indicators were also low compared to MLR (Table 3). However, the MAPE of the RWC for ANN (6.1%) was approximately as accurate as the values obtained from MLR with MAPE (7.7%). ANN and MLR models were run based on the training data set and another set of data was used to validate their performance. The correlation ( $R$ ) between MCI estimated with satellite data and MCI calculated using field data and aggregated Landsat products ranges between 0.85 and 0.97 for ETM+ and between 0.83 and 0.88 for MODIS ( $p < 0.001$  data not shown). Overall, the results

showed that the ANN method had a higher accuracy for the validation dataset (testing) in predicting and spatially mapping LFMC, RWC, LDMC, and DFMC for the study area. It can also be concluded that MCI estimation results from the ANN had better accuracy and generalization performance for the new data (validation dataset which is not in the training set) in comparison with MLR. Coefficients of determination ( $R^2$ ) showed that using the ANN method to predict MCIs (LFMC, LDMC, RWC, and DFMC) generates good precision ( $R^2$  ranges from 0.76 to 0.94 for ETM+) and also precision from MODIS ranges from 0.7 to 0.78 (in Table 3). The statistical accuracy assessment of ANN and MLR models for MCIs are summarized in Table 3.

**Table 3.** Accuracy assessment of MCI estimated with satellite images using ANN and MLR models with MCI calculated using field data and aggregated Landsat products. The validation results are shown in bolded numbers.

Estimated Indicators	Dataset	RMSE	MAE	MAPE	$R^2$
LFMC (ETM+)	Training (ANN)	14	11.3	7.6%	0.94
	<b>Validation (ANN)</b>	<b>15.6</b>	<b>12.6</b>	<b>5.9%</b>	
	Training (MLR)	19.9	15.4	9.82%	0.90
	Validation (MLR)	24.4	20.7	16.03%	
LFMC (MODIS)	Training (ANN)	43.4	31	26.63%	0.70
	<b>Validation (ANN)</b>	<b>48</b>	<b>33</b>	<b>29.25%</b>	
	Training (MLR)	47.1	34.6	30.21%	0.65
	Validation (MLR)	50.2	36.8	32.98%	
RWC (ETM+)	Training (ANN)	4.4	3.8	6%	0.94
	<b>Validation (ANN)</b>	<b>5.8</b>	<b>3.6</b>	<b>6.1%</b>	
	Training (MLR)	3.5	2.9	4.59%	0.90
	Validation (MLR)	6.4	5.1	7.77%	
RWC (MODIS)	Training (ANN)	7.3	4.5	7.84%	0.75
	<b>Validation (ANN)</b>	<b>8</b>	<b>5</b>	<b>8.58%</b>	
	Training (MLR)	7.6	5	8.87%	0.73
	Validation (MLR)	8.3	5.5	9.42%	
LDMC (ETM+)	Training (ANN)	2.5	1.9	8%	0.76
	<b>Validation (ANN)</b>	<b>2.2</b>	<b>1.8</b>	<b>7.7%</b>	
	Training (MLR)	2.2	1.7	7.14%	0.73
	Validation (MLR)	5.2	4.1	17.32%	
LDMC (MODIS)	Training (ANN)	4.8	2.9	11.19%	0.78
	<b>Validation (ANN)</b>	<b>4.6</b>	<b>2.9</b>	<b>11%</b>	
	Training (MLR)	5.4	3.7	14.41%	0.72
	Validation (MLR)	5.2	3.7	14.6%	
DFMC (ETM+)	Training (ANN)	1.7	2.5	12.67%	0.79
	<b>Validation (ANN)</b>	<b>3</b>	<b>2.2</b>	<b>12.2%</b>	
	Training (MLR)	2.8	2.2	14.43%	0.76
	Validation (MLR)	4.8	3.8	16.68%	
DFMC (MODIS)	Training (ANN)	2.17	1.4	9.6%	0.71
	<b>Validation (ANN)</b>	<b>2.6</b>	<b>1.7</b>	<b>12.1%</b>	
	Training (MLR)	2.45	1.7	11.6%	0.64
	<b>Validation (MLR)</b>	<b>2.9</b>	<b>1.99</b>	<b>13.9%</b>	

The structural similarity index used to compare the original 30 m MCI and aggregated 500 m MCI using nearest neighbor shows a value of 0.99 (high similarity between the two data sets). Comparison of residual standard errors between the aggregated (30 m–500 m) MCI and MCI estimated using MODIS data (500 m) are shown in Figure 3. The residual standard errors show that the spatial pattern of estimation of LFMC and RWC from MODIS 500 m, for both models (MLR and ANN) was almost the same (cream colored areas). However, the spatial pattern for LDMC and DFMC as calculated using MODIS and Landsat products for both MLR and ANN was dissimilar. For example, the value of DFMC in the northwestern corner of the study area indicated that the residual for the MLR model was notable, but near zero for the ANN model. In this case, zero means that the estimated DFMC equals the aggregated DFMC. Based on Figure 3 it can be concluded that both estimated MCI and aggregated MCI are fairly equivalent to  $-0.5$  to  $0.5$  residual standard errors (in cream colored area),

thus the scaling up approach adopted in this study is successful in preserving the spatial information of fuel moisture.

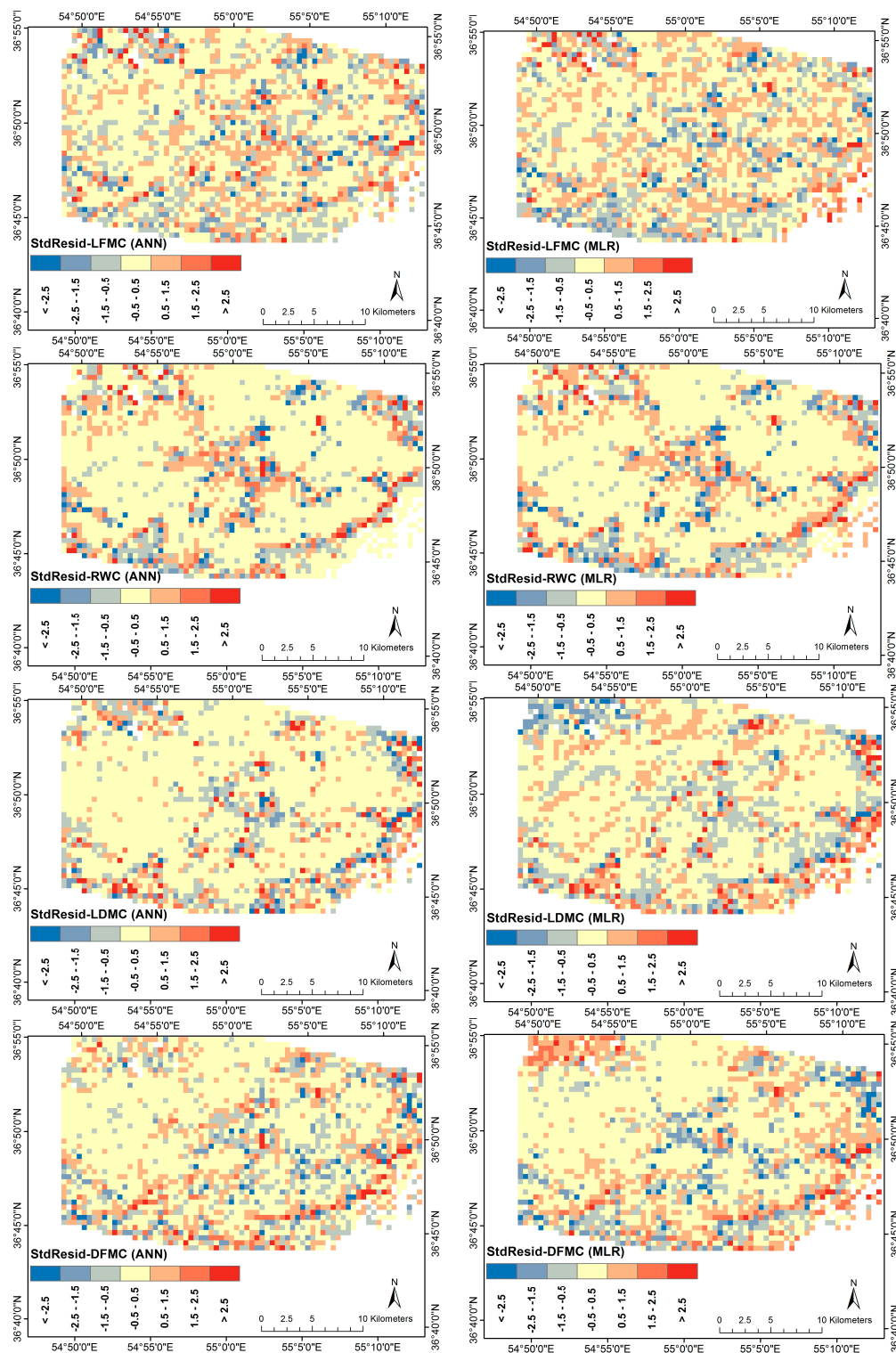


**Figure 3.** Visual comparison of residual standard errors between estimated LFM, RWC, LDMC, and DFMC from aggregated Landsat products and MODIS by MLR and ANN. Blue color shows the values estimated by MODIS was more than ETM+ (overestimates) and the brown color displays the values estimated by MODIS was less than ETM+ (underestimates). There were no differences between the value aggregated Landsat products and MODIS in cream colored area.

### 3.3. Scale Discrepancy between Plot and Satellite Data

The MCI indicators calculated using data collected in the field were correlated with various parameters extracted from MODIS satellite data that are commonly used in MCI estimation. This was done to investigate the scale discrepancy between plot and satellite data when plot data are directly correlated to coarse spatial resolution satellite data. It was found that the  $R^2$  became very low and non-significant when in-situ MCI measurements were directly matched to MODIS data ( $R^2$  for LDMC ranges between 5% and 41%, for LFMC 7%–36%, RWC 6%–33%, and DFMC 6%–22% data not shown). In contrast, there were high levels of correlation when the aggregated ETM+ derived MCI were linked to MODIS data ( $R^2$  for LDMC ranges between 15% and 72%, for LFMC 20%–67%, RWC 22%–67%, and DFMC 10%–50%). It is important to distinguish the influence of scale mismatch between the data collected on the ground and the 500 m MODIS data. The overall correlation analysis from the  $R^2$  showed that the aggregated ETM+ derived LDMC, LFMC, RWC and DFMC (500 m) was better correlated with the MODIS data (500 m) than the in-situ MCI measurements (30 m). Therefore, daily estimations of LDMC, LFMC, RWC and DFMC from MODIS data could be accurate if the aggregated MCI data were used in MLR and ANN models.

### 3.4. Mapping Leaf Moisture and Dry Matter Content (MCI) Using ETM+ Data

MCI (LFMC, RWC, LDMC, and DFMC) calculated from Landsat ETM+ (6 August 2010) using the ANN method is shown in Figure 4 (we only show the results of ANN as it yielded higher accuracy compared to MLR-Table 3). Lower values for LFMC, RWC and DFMC were found in the central region that was urbanized with relatively higher temperatures driving possibly dry live fuels, and northern slopes of the study area that are dominated by the south dry warm Foehn wind [58]. Dry warm Foehn wind is created by wind travelling from southern to northern slopes over the Alborz mountain range, which dries fuels and makes ideal conditions for rapid spread of fires in the forested area. The LFMC values were lower than 20% on the southern slopes where leaves on trees are generally considered to be dead (not live) because southern aspects receive more direct solar radiation and absorb more of the sun's heat, causing high temperatures and evapotranspiration, robust winds, and low air humidity [59] which results in low vegetation density and lower fuel moisture contents.

If live fuel moisture drops below 30%, the fuel is considered fully cured (no live fuel) [60]. Figure 4 shows some low values (1.3%–29%) of LFMC (only 7% of the entire study area) that could be due to the nonlinear statistical technique (ANN) used in this study. A nonlinear relationship exists between vegetation indices/atmospheric variables and MCI and, consequently, low values of MCIs could be inadequately predicted or perhaps undetected by the model, these similar problems were also encountered by Chuvieco, et al. [22], Chuvieco, et al. [61], and Dennison, et al. [29]. This is also the case for the Caspian Hyrcanian Forests ecoregion in the early fall. The increase of rainfall on the north slopes of the mountain ranges of the Alborz [62] can increase dead fine fuels' moisture content while the effect of rainfall on dead fine fuel moisture content is quite a complex process [63]. For example, less rain could be absorbed by dead fine fuel when initial moisture content in fuel is high [64]. Dead (forest understory) fuels contain a range of moisture with the highest values on the north slope position and the lowest value on the south slope of the study area because south slopes were hotter and drier than north slopes. In the valley bottoms of the study area, DFMC was high because nocturnal air temperatures were coolest and humidity was highest. Aspects created heterogeneous dead fuel moistures across the study area. Live fuel moisture with low LDMC (the ratio of leaf dry mass to turgid mass) generally corresponds with dry mass of the live leaf and therefore, areas with high levels of dry matter were found in the central and surrounding regions where both LFMC and RWC were low. These results show that the material in the central region and surrounding regions of the study area were more prone to combustion as the moisture content in the live fuels was low because leaves were dead on the canopy (LFMC is lower than 30%).

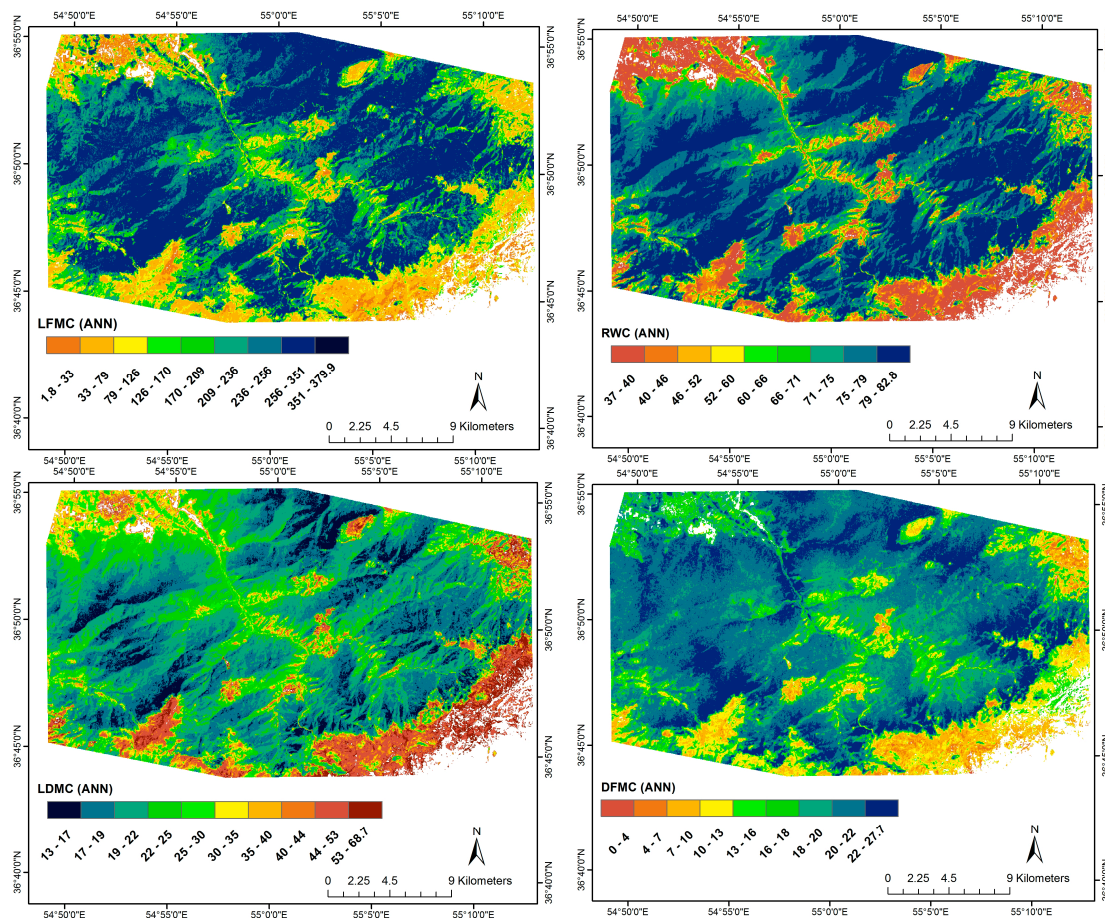


**Figure 4.** Estimated LFMC, RWC, LDMC, and DFMC (%) from ETM+ (30 m) using the ANN technique for the Zaringol forest at 11:20 a.m. local time, on 6 August 2012.

### 3.5. Mapping Leaf Moisture and Dry Matter Content (MCI) Using MODIS Data

The four MCIs that were derived using upscaled data from 6 August 2012 are shown in Figure 5. The results show that the spatial pattern of MODIS derived MCIs (500 m) were mostly similar as Landsat ETM+ (30 m) but the range of values were slightly different. For example, the range of values estimated by ANN for DFMC using ETM+ data were between 0% and 27% but for MODIS, these values ranged from 7% to 23%. According to Figures 4 and 5, the visual interpretation confirms that MCIs classes (pattern) were clearly discriminated in ETM+ and MODIS data by the ANN method. Taking into account the statistical result, the Pearson correlation ( $R$ ) between the aggregated ETM+ MCIs products at 500 m (i.e., using the nearest neighbor pixel of ETM+ MCI products) and derived independent data from MODIS data at 500 m (i.e., vegetation indices and biophysical variables) for estimating values of MCIs by ANN and MLR showed a good fit for all MCI with  $R$  ranging between 0.8–0.85 for MLR and 0.83–0.88 for ANN. However, upscaled 500 m MODIS MCIs generated from ANN method presents higher accuracy than the MLR method with an overall  $R$  value of 0.85.

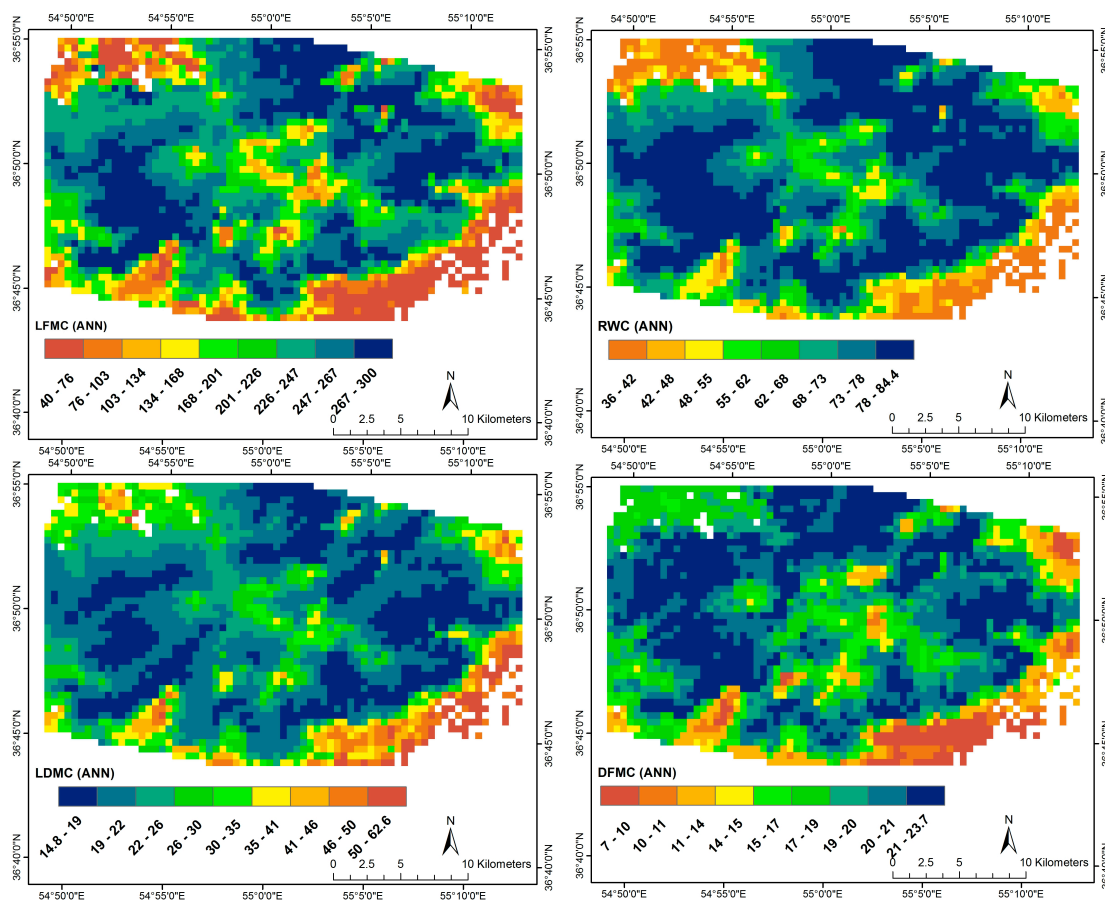


**Figure 5.** The MCI data (%) upscaled from 30 m Landsat ETM+ to the spatial resolution of the Terra MODIS (500 m) using ANN technique for the Zaringol forest at 11:40 a.m. local time, on 6 August 2012.

#### 4. Discussion

Optical remote sensing can effectively be used for estimating MCI because water influences spectral reflectance through absorption of radiation within the near infrared and shortwave infrared regions [65]. Thus, vegetation reflectance increases throughout the visible, NIR and MIR regions under water stress conditions and vegetation indices have been developed using spectral bands to quantify water content in vegetation [66]. In this study, we found that the spectral vegetation indices and biophysical and atmospheric variables from ETM+ and MODIS remote sensing data were moderately related to leaf moisture (LFMC, RWC, DFMC) and leaf dry content (LDMC) in each 30 by 30 m plot. Spectral vegetation indices were highly correlated with LFMC ( $R^2$  60%) RWC ( $R^2$  62%), and LDMC ( $R^2$  65%) (Section 3.3). This means that the multi reflectance data from different wavelength regions (i.e., from visible to thermal infrared) were sensitive to the moisture content in a leaf and so could be used for estimating LFMC [67]. The major seasonal variation in leaf moisture content is related to precipitation, air relative humidity, air and surface temperature, wind, and cloud, as well as by fuel factors such as surface to volume ratio, compactness, and arrangement [68]. RWC has been shown to significantly increase from summer drought to winter in Mediterranean woody species [11] which shows that water stress significantly reduces the RWC due to cellular degradation of the leaf [69]. Dead fuel moisture depends on time and weather variables such as temperature, atmospheric relative humidity, incoming solar radiation and precipitation [25]. Soil moisture also can prevent temperature increases at the land surface that influences dead fuel moisture above ground [70].

Estimation of dead fuel moisture content (DFMC) is important in the case of Zaringol forest because most of the fires here are surface fires. However, estimation of DFMC from optical remote

sensing data is difficult because at moderate/coarse spatial resolutions of 30 m/500 m there is a mixture of live vegetation, dead vegetation, soil, bark, rock, shadows, etc. that can influence the spectral reflectance. This means that pixels have mixed reflectance information from different land types on low-spatial-resolution data such as MODIS (1 km<sup>2</sup> at nadir). Although vegetation indices such as SLAVI and the Normalized Canopy Index (NCI) can minimize the effects of soil (SLAVI) and the effects caused by changes in the angle of the sun, atmosphere, canopy background, topography and soil variations [71] the issue of mixed pixels could be the reason for the poor relationship between the spectral indices (e.g., Albedo) and DFMC ( $R^2$  10%). In this study, up-scaling is used as a method to minimize mixed pixels that in turn results in higher accuracy of DFMC at the coarser resolution such as MODIS. Moreover, water interactions with dead fuels are complex (i.e., water vapor pressure difference between the atmosphere and fuel particle) [72] and difficult to generalize from individual dead fuel samples directly, especially when the canopy cover is high (high leaf area index) and causes large shaded areas such that dead fuels are shaded from direct solar radiation. Therefore it is difficult to generalize and estimate DFMC in shaded areas. Other studies such as that of Finney [73] found that LAI and surface reflectance influenced DFMC because leaves of broadleaf forests can create full leaf shadows (high LAI) for the dead fuels on the ground that in turn increases the amount of moisture in a fuel. This may be one of the reasons for the high correlation between LAI and DFMC, as found in this study (Section 3.3). In this study, the relative humidity (RH) was the fourth most significant variable that influenced moisture content in dead fuels ( $R = 0.48$ ). This was similar to the findings of Nolan, et al. [74] who found a strong link between vapor pressure deficit and DFMC (MAE was less than 5.0%). Dead fuel dries out during times when relative humidity is low because the fuel moisture is removed from leaves to the atmosphere. Increasing vegetation cover causes reduced solar radiation and reduced turbulent mixing between the forest floor and the atmosphere which produces lower air temperatures and higher levels of humidity and therefore higher fuel moisture [75].

The LDMC was found to decrease as LAI increased ( $R = -0.83$ ). This is similar to other studies which shows a negative relationship between LDMC and LAI [76]. It was also observed that the moisture content of leaf litter in the forest understory could be estimated by LAI obtained using remotely sensed data due to buffering effect of LAI on the understory microclimate [77]. Forest interiors often cause slightly different local microclimates and disturbance regimes than forest edges because dense vegetation reduces incoming solar radiation, reducing mean ambient temperatures wind, and many types of environmental disturbances [78].

Fuel moisture content has been estimated using statistical/empirical methods and physical model based approaches (Table 1). In a previous study, Sharples and Matthews [27], Merzouki and Leblon [79], Lin [24], and Aguado, et al. [26] used LR models to estimate litter and duff moisture, while in the present study, ANN models have had a superior performance, with Pearson correlation coefficients of 0.8 for MODIS and 0.89 for ETM+ data (Table 1). Estimation of other indicators such as RWC and LDMC has not been commonly attempted using remote sensing data and the result of this study shows that satellite remote sensing data can be used to fill these gaps. ANN modelling estimated RWC and LDMC with a Pearson correlation coefficients of 0.86 and 0.88, respectively, for upscaled MODIS and ETM+ products. The ANN model greatly improved the accuracy of LFMC estimates ( $R$  of 0.97 for ETM+ and 0.83 for MODIS data) compared to previous studies such as that of Qi, et al. [37], Sow, et al. [38], Verbesselt, et al. [30], and Dasgupta, et al. [31] who yielded  $R = 0.49, 0.63, 0.75,$  and  $0.54,$  respectively, with a LR model (Table 1).

Empirical methods for LFMC and DFMC estimation are commonly based on statistical fitting between field-measured LFMC and spectral measures based on reflectance of remote sensing data (Table 1). In this study, since ANNs provided a more accurate prediction of MCI than MLR, we conclude that MCI have nonlinear pattern with spectral information of remote sensing data. Most of the previous studies have used linear regression methods to estimate LFMC, however, as shown in the accuracy assessment, the ANN technique was also more stable to new data (validation data) than MLR. This is due to the fact that vegetation indices (i.e., Normalized Dry Matter Index, Dry Matter Content Index,

Normalized Difference Water Index and Normalized Difference Infrared Index) have a non-linear and polynomial trend relationships with LFMC [80] and ANNs are able to compute any function for estimating MCI because the relationship between input data and output data can be non-linear, whereas the MLR model cannot identify these non-linear relationships. Although empirical models such as MLR are easy to use and can be applied to a large temporal dataset [24,27,37,38], they have a serious limitation of not being able to capture nonlinear relationships in the data. ANNs have been found to produce lower errors of estimation (e.g., fuel moisture content) than linear regression [57,81]. There were nonlinear associations between MCIs and PC1, PC2, Varimax1 and Varimax2 ( $p$ -value for curvature  $<0.001$ ). The error of estimation of any empirical model is important; for example, an error of  $\pm 20\%$  added to 90% of estimated LFMC changed the fire danger of shrub land from low to high [82]. In this study, the estimated MCI using ETM+ satellite data and ANN technique was closer to the actual value obtained from in-situ data (MAPE  $< 12\%$ ). This implies that fire danger can be predicted with reasonable accuracy as previous studies by Chuvieco et al. [83] and Chuvieco et al. [22] showed an error of 23% for both Landsat Thematic Mapper, and AVHRR data in LFMC estimation of woodlands, and grassland/shrubland. However, sensitivity analysis must be performed in future to test the effect of different degree of errors in MCI for predicting fire danger.

Nevertheless, differences in vegetation bio-physical characteristics over a large area make extrapolating from a single site to regional or global scale using empirical methods problematic [84]. Therefore, several studies have formulated and used radiative transfer models (RTM) [85,86] to estimate fuel moisture. A performance comparison of statistical and physical approaches to derive LFMC in the Mediterranean shrubland and grassland species from MODIS reflectance data have shown that both methods produce good estimates of LFMC. The RTM produced lower standard errors of estimation compared to the statistical fitting methods [34], nevertheless, the RTM is based on simulated data and therefore intensive computing is required and it is more complex to extract parameters and characteristics of actual canopy [87,88] than statistical methods but RTMs have the ability to simulate actual canopy characteristics for use in realistic terrestrial environments [88]. Clearly, soft computing approaches including ANN can offer more flexible equations since they allow us to use non-linear prediction ability and the generalization ability to create models for finding the best fit model between the measured and modelled MCI, and therefore these methods offer better generality than traditional techniques. Statistical models such as partial least square regression (PLSR), principal component regression (PCR), Bayesian model averaging or spectral un-mixing approaches are also easy to apply [89] and they will be explored in future studies.

The type of satellite sensors and their spatial resolutions used to estimate fuel moisture content is an important consideration for any method (either empirical or physical). Table 1 summarizes some examples of the applications of remote sensing data for various fuel moisture indices. Most of the studies are focused on high temporal resolution sensors such as AVHRR and MODIS. Medium-spatial-resolution sensors such as Landsat Thematic Mapper (TM), Enhanced Thematic Mapper + (ETM+), SPOT Veg and IRS sensors have also been used to estimate LFMC because they contain more spatial detail of fuel moisture compared to the coarse spatial resolution images of MODIS and AVHRR [83,90]. Although Chuvieco et al. [61] found a slightly stronger correlation between field-measured LFMC and vegetation indices calculated from Landsat TM data compared to AVHRR and SPOT-Vegetation, the poor temporal revisit time of Landsat satellite (16 days) limits its use for forest fire monitoring purposes.

In this study, LFMC calculated from the Landsat ETM+ image resulted in higher mean absolute accuracy (MAE 13%) compared to MODIS data (MAE 33%) (Table 3). It was shown that the MAE for LFMC of 8%–23% was acceptable for fire danger applications [83]. As the spectral properties of leaves change due to seasonal variation, moisture in vegetation also changes. In this study, our model was applied on one day of the warm season (fire season) so it cannot be used for estimating MCI on a cold season. Our model was developed based on satellite data which was acquired around midday, so the model cannot be used in the early morning or late afternoon hours as it may introduce some

noise such as time discrepancy between biomass burning and MCIs satellite data. Therefore, the error (MAPE 7%–29%) associated with MODIS data may make it unsuitable for fire danger applications for Caspian Hyrcanian forest since tree species in this forest are more variable throughout the year.

## 5. Conclusions

Estimation of fuel moisture based on remote sensing data have so far focused on live fuels, but is less commonly used to estimate dead fuel moisture. In this study, both live and dead fuel moisture were estimated using medium (low temporal) and coarse spatial (high temporal) resolutions of Landsat ETM+ and MODIS satellite data for a temperate humid forest in northeastern Iran. More specifically, the leaf water-related properties (LFMC, RWC, DFMC) and leaf dry matter content (LDMC) were calculated in the field using leaf samples collected from 32 trees, representing eight different species. These data and remotely sensed indices (vegetation, atmospheric and biophysical) were calculated using ETM+ and MODIS data and used to estimate the MCI of Zaringol forest by empirical models (i.e., Multiple Linear Regression (MLR) and Artificial Neural Network (ANN)). The ANN method had an overall mean predictive absolute error of less than 15% for all four up-scaled MCI in the validation data set compared to the MLR with 18%. The ANN was found to be a robust statistical method to upscale MCI. These MCI did not show any significant inter-species differences. We have shown that MCI can be monitored and upscaled across large spatial areas using statistical methods. Moreover, the temporal upscaling procedure (with MODIS) developed and used in this research showed promising results for instantaneous (near real time) monitoring of live and dead leaves (fuel) moisture in temperate zones and the proposed methodology can be used on larger areas with similar climatic and geographic conditions (i.e., Caspian Hyrcanian forest ecoregion) in the warm season. The method which was developed using empirical relationships between spectral-biophysical indices calculated using remote sensing data and MCI using ground data may not be suitable for a regional or global scale mapping. This is due to the spatially varying leaf and canopy characteristics, soil background, climatic conditions, etc. In previous studies (Table 1), researchers usually developed methods to estimate fuel moisture for small areas with limited regional/global database. For regional or global scale moisture content indices (MCI) mapping, it is necessary to have a global field measurements network. Estimating MCI from remotely sensed data is a difficult task because it is dependent on several parameters such as the physical properties of leaves and background soil that can influence the accuracy of the MCI estimations. However, remote sensing data provide an easy and useful spectral and atmospheric basis for estimating MCI on different spatial and temporal scales, especially when used together with the approach adopted in this research. Improved spatial and temporal monitoring of MCI using remote sensing data (result of this study) can assist forestry organizations and the general public on the risk of fire occurrences and to better manage fire protective resources in fire prone landscapes. Future studies can focus on developing MCI estimated using remotely sensed data into fire risk assessment for operational fire monitoring. Our future study will focus on developing an operational daily fire susceptibility index (during the fire season in Zaringol forest) using information related to live and dead leaves for various tree species in the forest of Zaringol at a spatial resolution of 500 m and using Rothermel's pre-ignition heat function.

**Acknowledgments:** We acknowledge the Ministry of Education Malaysia (through research grant Q.J130000.2427.02G20 and Q.J130000.2527.13H44) for providing funding to conduct the study. Beringer is funded under an ARC Future Fellowship (FT110100602).

**Author Contributions:** Hamed Adab designed the research and wrote the manuscript; Kasturi Devi Kanniah supervised the research and wrote the manuscript; Jason Beringer reviewed and edited the manuscript.

**Conflicts of Interest:** The authors declare no conflict of interest.

## Appendix A

**Table A1.** Descriptions of variables potentially related to MCI indicators of humid temperate forest in Iran. Variables used to estimate LFMC, LDMC, RWC are marked as \* and variables used to estimate DFMC are marked as #.

<b>Biophysical Indices and Atmospheric Variables</b>	
* # Leaf Area Index (LAI) <sub>ETM+</sub> = 0.57 exp (2.33NDVI)	[91]
* # LAI <sub>MODIS</sub> = [NDVI × (1 + NDVI) / (1 - NDVI)] <sup>0.5</sup>	[92]
* # Albedo <sub>ETM+</sub> = 0.356ρ <sub>1</sub> + 0.130ρ <sub>3</sub> + 0.373ρ <sub>4</sub> + 0.085ρ <sub>5</sub> + 0.072ρ <sub>7</sub> - 0.0018	[93,94]
* # Albedo <sub>MODIS</sub> = 0.160ρ <sub>1</sub> + 0.291ρ <sub>2</sub> + 0.243ρ <sub>3</sub> + 0.116ρ <sub>4</sub> + 0.112ρ <sub>5</sub> + 0.081ρ <sub>7</sub> - 0.0015	[94]
* # LST <sub>ETM+</sub> = $\frac{K_2}{\ln\left(\frac{K_1}{CV_{R2}} + 1\right)}$	[95]
* # LST <sub>MODIS</sub> = btm31 + 1.02 + 1.79 × (btm31 - btm32) + 1.2 × (btm31 - btm32) <sup>2</sup> + (34.83 - 0.68 × W) × (1 - e) + (-73.27 - 5.19 × W) × de	[50]
* # T <sub>a</sub> = T <sub>s</sub> - $\left(\frac{H_{raH}}{\rho_{AIR}C_p}\right)$	[96]
* # Relative Humidity (RH) = α((bx <sub>1</sub> + c) <sup>2</sup> + (dx <sub>2</sub> + e) <sup>2</sup> )	[97]
<b>Vegetation Indices</b>	
* Specific Leaf Area Vegetation Index (SLAVI) = $\frac{\rho_{NIR}}{(\rho_{RED} + \rho_{SWIR2})}$	[71]
* Normalized Difference Infrared Index (NDII) = $\frac{(\rho_{NIR} - \rho_{SWIR2})}{(\rho_{NIR} + \rho_{SWIR2})}$	[30]
* Normal Difference Water Index (NDWI) = $\frac{(\rho_{NIR} - \rho_{SWIR1})}{(\rho_{NIR} + \rho_{SWIR1})}$	[34]
* Normalized Canopy Index (NCI) = $\frac{(\rho_{SWIR1} - \rho_{GREEN})}{(\rho_{SWIR1} + \rho_{GREEN})}$	[71]
* Visible Atmospherically Resistant Index (VARINIR) = $\frac{(\rho_{NIR} - \rho_{RED})}{(\rho_{NIR} + \rho_{RED} - \rho_{BLUE})}$	[21]
* Green - Blue NDVI (GBNDVI) = $\frac{NIR - (\rho_{GREEN} + \rho_{BLUE})}{NIR + (\rho_{GREEN} + \rho_{BLUE})}$	[98]
* NDVI = $\frac{(\rho_{NIR} - \rho_{RED})}{(\rho_{NIR} + \rho_{RED})}$	[30]
* Optimal Soil Adjusted Vegetation Index (OSAVI) = $\frac{(\rho_{NIR} - \rho_{RED})}{(\rho_{NIR} + \rho_{RED} + L)}$	[65]
* Normalized Difference Infrared Index (NDII) = $\frac{(\rho_{NIR} - \rho_{SWIR2})}{(\rho_{NIR} + \rho_{SWIR2})}$	[35]

Abbreviations: ρ<sub>i</sub> is equal to corrected reflectance of each band, CV<sub>R2</sub> is the atmospherically corrected spectral radiance in W/(m<sup>2</sup>·ster·μm) and K<sub>2</sub> and K<sub>1</sub> are pre-launch calibration constants. For LANDSAT 7 ETM+, K<sub>2</sub> = 1282.71 K, and K<sub>1</sub> = 666.09 mW·cm<sup>-2</sup>·sr<sup>-1</sup>·μm<sup>-1</sup> [49], btm31 = brightness temperature obtained from MODIS band 31, btm32 = brightness temperature obtained from MODIS band 32, W = Water vapor content (The MODIS product (MOD 05) consists of column water-vapor amounts at the 1 km spatial resolution of the near-infrared), e = Surface emissivity, de = Surface emissivity. T<sub>a</sub> = Air temperature (K), H = Sensible Heat Flux (W·m<sup>-2</sup>), ρ<sub>AIR</sub> = Density of Air humidity (1.27 kg·m<sup>-3</sup>), C<sub>p</sub> = Air specific heat in constant pressure (~1004 J·Kg<sup>-1</sup>·K<sup>-1</sup>), T<sub>s</sub>=Surface temperature (K), H<sub>raH</sub> = Aerodynamic resistance (sm<sup>-1</sup>). RH = air relative humidity (percent), x<sub>1</sub> = elevation (meter), x<sub>2</sub> = downscaled water vapor in Near-Infrared of MODIS (g·cm<sup>-2</sup>), a: 4.03, b: -0.001, c: 3.34, d: -0.35, e: 3.04. L = soil brightness correction factor.

## Abbreviations

The following abbreviations are used in this manuscript:

ARND	Accumulated Relative NDVI Decrement
ETM+	Enhanced Thematic Mapper Plus
GVMI	Global Vegetation Moisture Index
IM	Inversion Models
IRS	Infra-Red Scanner (HJ-1B IRS)
IVDI	Improved VDI
LOPEX	Leaf Optical Properties Experiment
LR	Linear Regression
LST	Land Surface Temperature
MSI	Moisture Stress Index
MCI	Moisture Content Index
MODIS	MODerate-resolution Imaging Spectroradiometer

NDII	Normalized Difference Infrared Index
NDVI	Normalized Difference Vegetation Index
NDWI	Normalized Difference Water Index
RGRE	Relative Greenness
SIWSI	Shortwave Infrared Water Stress Index
SPOT	Satellites Pour l'Observation de la Terre or Earth-observing Satellites
SRWI	Simple Ratio Water Index
TM	Landsat Thematic Mapper
VARI	Visible Atmospheric Resistant Index
VDI	Vegetation Dryness Index

## References

- Papió, C.; Trabaud, L. Structural characteristics of fuel components of five mediterranean shrubs. *For. Ecol. Manag.* **1990**, *35*, 249–259. [[CrossRef](#)]
- Bisquert, M.; Sánchez, J.M.; Caselles, V. Modeling fire danger in Galicia and Asturias (Spain) from MODIS images. *Remote Sens.* **2014**, *6*, 540–554. [[CrossRef](#)]
- Silva, D.M.; Batalha, M.A.; Cianciaruso, M.V. Influence of fire history and soil properties on plant species richness and functional diversity in a neotropical savanna. *Acta Bot. Bras.* **2013**, *27*, 490–497. [[CrossRef](#)]
- Brady, M.A.; de Groot, W.J.; Goldammer, J.G.; Keenan, T.; Lynham, T.J.; Justice, C.O.; Csiszar, I.A.; O'Loughlin, K. Developing a global early warning system for wildland fire. In *Managing Weather and Climate Risks in Agriculture*; Sivakumar, M.V.K., Motha, R.P., Eds.; Springer: Berlin, Germany, 2007; pp. 355–366.
- Chowdhury, E.H.; Hassan, Q.K. Development of a new daily-scale forest fire danger forecasting system using remote sensing data. *Remote Sens.* **2015**, *7*, 2431–2448. [[CrossRef](#)]
- De Groot, W.J.; Goldammer, J.G.; Keenan, T.; Brady, M.A.; Lynham, T.J.; Justice, C.O.; Csiszar, I.A.; O'Loughlin, K. Developing a global early warning system for wildland fire. *For. Ecol. Manag.* **2006**, *234*, S10. [[CrossRef](#)]
- Grassein, F.; Till-Bottraud, I.; Lavorel, S. Plant resource-use strategies: The importance of phenotypic plasticity in response to a productivity gradient for two subalpine species. *Ann. Bot.* **2010**, *106*, 637–645. [[CrossRef](#)] [[PubMed](#)]
- Davies, G.; Legg, C. Fuel moisture thresholds in the flammability of *calluna vulgaris*. *Fire Technol.* **2011**, *47*, 421–436. [[CrossRef](#)]
- Viegas, D.X.; Piñol, J.; Viegas, M.T.; Ogaya, R. Estimating live fine fuels moisture content using meteorologically-based indices. *Int. J. Wildland Fire* **2001**, *10*, 223–240. [[CrossRef](#)]
- Pausas, J.G.; Paula, S. Fuel shapes the fire–climate relationship: Evidence from mediterranean ecosystems. *Glob. Ecol. Biogeogr.* **2012**, *21*, 1074–1082. [[CrossRef](#)]
- Saura-Mas, S.; Lloret, F. Leaf and shoot water content and leaf dry matter content of mediterranean woody species with different post-fire regenerative strategies. *Ann. Bot.* **2007**, *99*, 545–554. [[CrossRef](#)] [[PubMed](#)]
- Cornelissen, J.H.C.; Lavorel, S.; Garnier, E.; Díaz, S.; Buchmann, D.N.; Gurvich, D.E.; Reich, P.B.; Steege, H.T.; Morgan, H.D.; van der Heijden, M.G.A.; et al. A handbook of protocols for standardised and easy measurement of plant functional traits worldwide. *Aust. J. Bot.* **2003**, *51*, 335–380. [[CrossRef](#)]
- Marino, E.; Dupuy, J.-L.; Pimont, F.; Guijarro, M.; Hernando, C.; Linn, R. Fuel bulk density and fuel moisture content effects on fire rate of spread: A comparison between firetec model predictions and experimental results in shrub fuels. *J. Fire Sci.* **2012**, *30*, 277–299. [[CrossRef](#)]
- Rachmilevitch, S.; DaCosta, M.; Huang, B. Physiological and biochemical indicators for stress tolerance. In *Plant-Environment Interactions*, 3rd ed.; CRC Press: Boca Raton, FL, USA, 2006; pp. 321–355.
- Zhang, J.; Wu, J.; Zhou, L. Retrieval of fuel moisture content from hyperspectral data via partial least square. In Proceedings of the 2010 IEEE International Geoscience and Remote Sensing Symposium, Honolulu, HI, USA, 25–30 July 2010.
- Yool, S. Broad-scale monitoring of live fuel moisture. *Geogr. Compass* **2009**, *3*, 1703–1716. [[CrossRef](#)]
- Dimitrakopoulos, A.P.; Bemmerzouk, A.M.; Mitsopoulos, I.D. Evaluation of the canadian fire weather index system in an eastern mediterranean environment. *Meteorol. Appl.* **2011**, *18*, 83–93. [[CrossRef](#)]
- Ghulam, A.; Qin, Q.; Teyip, T.; Li, Z.-L. Modified perpendicular drought index (MPDI): A real-time drought monitoring method. *ISPRS J. Photogramm. Remote Sens.* **2007**, *62*, 150–164. [[CrossRef](#)]

19. Wang, L.; Qu, J.J.; Zhang, S.; Hao, X.; Dasgupta, S. Soil moisture estimation using MODIS and ground measurements in Eastern China. *Int. J. Remote Sens.* **2007**, *28*, 1413–1418. [[CrossRef](#)]
20. Hassan, Q.; Bourque, C.; Meng, F.-R.; Cox, R. A wetness index using terrain-corrected surface temperature and normalized difference vegetation index derived from standard MODIS products: An evaluation of its use in a humid forest-dominated region of Eastern Canada. *Sensors* **2007**, *7*, 2028–2048. [[CrossRef](#)]
21. Schneider, P.; Roberts, D.A.; Kyriakidis, P.C. A vari-based relative greenness from MODIS data for computing the fire potential index. *Remote Sens. Environ.* **2008**, *112*, 1151–1167. [[CrossRef](#)]
22. Chuvieco, E.; Aguado, I.; Cocero, D.; Riaño, D. Design of an empirical index to estimate fuel moisture content from NOAA-AVHRR images in forest fire danger studies. *Int. J. Remote Sens.* **2003**, *24*, 1621–1637. [[CrossRef](#)]
23. Hufkens, K.; Bogaert, J.; Dong, Q.; Lu, L.; Huang, C.; Ma, M.; Che, T.; Li, X.; Veroustraete, F.; Ceulemans, R. Impacts and uncertainties of upscaling of remote-sensing data validation for a semi-arid woodland. *J. Arid Environ.* **2008**, *72*, 1490–1505. [[CrossRef](#)]
24. Lin, C.C. Modeling fine dead fuel moisture in Taiwan Red Pine Forests. *Taiwan J. For. Sci.* **2004**, *19*, 27–33.
25. Weise, D.R.; Fujioka, F.M.; Nelson, R.M., Jr. A comparison of three models of 1-h time lag fuel moisture in Hawaii. *Agric. For. Meteorol.* **2005**, *133*, 28–39. [[CrossRef](#)]
26. Aguado, I.; Chuvieco, E.; Borén, R.; Nieto, H. Estimation of dead fuel moisture content from meteorological data in mediterranean areas. Applications in fire danger assessment. *Int. J. Wildland Fire* **2007**, *16*, 390–397. [[CrossRef](#)]
27. Sharples, J.J.; Matthews, S. Evaluation of some simplified models for predicting the moisture content of fine, dead fuels. In Proceedings of the 19th International Congress on Modelling and Simulation, Perth, Australia, 2011; pp. 242–248.
28. Danson, F.; Bowyer, P. Estimating live fuel moisture content from remotely sensed reflectance. *Remote Sens. Environ.* **2004**, *92*, 309–321. [[CrossRef](#)]
29. Dennison, P.E.; Roberts, D.A.; Peterson, S.H.; Rechel, J. Use of normalized difference water index for monitoring live fuel moisture. *Int. J. Remote Sens.* **2005**, *26*, 1035–1042. [[CrossRef](#)]
30. Verbesselt, J.; Somers, B.; Lhermitte, S.; Jonckheere, I.; van Aardt, J.; Coppin, P. Monitoring herbaceous fuel moisture content with spot vegetation time-series for fire risk prediction in savanna ecosystems. *Remote Sens. Environ.* **2007**, *108*, 357–368. [[CrossRef](#)]
31. Dasgupta, S.; Qu, J.J.; Hao, X.; Bhoi, S. Evaluating remotely sensed live fuel moisture estimations for fire behavior predictions in Georgia, USA. *Remote Sens. Environ.* **2007**, *108*, 138–150. [[CrossRef](#)]
32. Stow, D.; Niphadkar, M. Stability, normalization and accuracy of MODIS-derived estimates of live fuel moisture for Southern California chaparral. *Int. J. Remote Sens.* **2007**, *28*, 5175–5182. [[CrossRef](#)]
33. Yunhao, C.; Jing, L.; Guangxiong, P. Forest fire risk assessment combining remote sensing and meteorological information. *N. Z. J. Agric. Res.* **2007**, *50*, 1037–1044. [[CrossRef](#)]
34. Yebra, M.; Chuvieco, E.; Riaño, D. Estimation of live fuel moisture content from MODIS images for fire risk assessment. *Agric. For. Meteorol.* **2008**, *148*, 523–536. [[CrossRef](#)]
35. Peterson, S.H.; Roberts, D.A.; Dennison, P.E. Mapping live fuel moisture with MODIS data: A multiple regression approach. *Remote Sens. Environ.* **2008**, *112*, 4272–4284. [[CrossRef](#)]
36. Todone, F.; Bianchi, L.O.; Defossé, G.E. *First Field Sampling Results of Dead and Live Fuel Moisture Prediction in Patagonia*; Internal Report IR3.157b of the Integrated Project “Fire Paradox”, Project No. FP6-18505; European Commission: Patagonia, Argentina, 2009.
37. Qi, Y.; Dennison, P.; Spencer, J.; Riaño, D. Monitoring live fuel moisture using soil moisture and remote sensing proxies. *Fire Ecol.* **2012**, *8*, 71–87. [[CrossRef](#)]
38. Sow, M.; Mbow, C.; Hély, C.; Fensholt, R.; Sambou, B. Estimation of herbaceous fuel moisture content using vegetation indices and land surface temperature from MODIS data. *Remote Sens.* **2013**, *5*, 2617–2638. [[CrossRef](#)]
39. Li, L.; Ustin, S.L.; Riano, D. Retrieval of fresh leaf fuel moisture content using genetic algorithm partial least squares (GA-PLS) modeling. *IEEE Geosci. Remote Sens. Lett.* **2007**, *4*, 216–220. [[CrossRef](#)]
40. Zhang, J.; Wu, J.; Zhou, L. Deriving vegetation leaf water content from spectrophotometric data with orthogonal signal correction-partial least square regression. *Int. J. Remote Sens.* **2011**, *32*, 7557–7574. [[CrossRef](#)]
41. Farzipour, B. *Climate Change Impacts on Forest Fires in Iran*; University of Toronto: Toronto, ON, Canada, 2011.
42. Allard, G.B. *The Fire Situation in Islamic Republic of Iran*; FAO, Forestry Department: Rome, Italy, 2001.

43. Adab, H.; Kanniah, K.D.; Solaimani, K.; Sallehuddin, R. Modelling static fire hazard in a semi-arid region using frequency analysis. *Int. J. Wildland Fire* **2015**, *24*, 763–777. [[CrossRef](#)]
44. Sagheb-Talebi, K.; Sajedi, T.; Yazdian, F. *Forests of Iran*; Research Institute of Forests and Rangelands: Tehran, Iran, 2004.
45. Desbois, N.; Deshayes, M.; Beudoin, A. Protocol for fuel moisture content measurements. In *A Review of Remote Sensing Methods for the Study of Large Wildland Fires*; Chuvieco, E., Ed.; Universidad de Alcalá: Alcalá de Henares, Spain, 1997; pp. 61–72.
46. Garnier, E.; Shipley, B.; Roumet, C.; Laurent, G. A standardized protocol for the determination of specific leaf area and leaf dry matter content. *Funct. Ecol.* **2001**, *15*, 688–695. [[CrossRef](#)]
47. Pinto, A.; Espinosa-Prieto, J.; Rossa, C.; Matthews, S.; Loureiro, C.; Fernandes, P.M. Modelling fine fuel moisture content and the likelihood of fire spread in blue gum (*Eucalyptus globulus*) litter. In *VII International Conference on Forest Fire Research*; Imprensa da Universidade de Coimbra: Coimbra, Portugal, 2014; pp. 353–359.
48. Rego, F.; Moreira, F.; João Maia, M.; Catry e Conceição Colaço, F. *Fire Paradox: An Innovative Approach of Integrated Wildland Fire Management Regulating the Wildfire Problem by the Wise Use of Fire: Solving the Fire Paradox*; Instituto Superior De Agronomia: Lisboa, Portugal, 2010.
49. Barsi, J.A.; Schott, J.R.; Palluconi, F.D.; Hook, S.J. Validation of a web-based atmospheric correction tool for single thermal band instruments. *Proc. SPIE* **2005**. [[CrossRef](#)]
50. Sobrino, J.A.; El Kharraz, J.; Li, Z.L. Surface temperature and water vapour retrieval from MODIS data. *Int. J. Remote Sens.* **2003**, *24*, 5161–5182. [[CrossRef](#)]
51. Tonooka, H. Atmospheric correction of MODIS thermal infrared bands by water vapor scaling method. *Proc. SPIE* **2005**. [[CrossRef](#)]
52. Maxwell, S.K.; Schmidt, G.L.; Storey, J.C. A multi-scale segmentation approach to filling gaps in Landsat ETM+ SLC-off images. *Int. J. Remote Sens.* **2007**, *28*, 5339–5356. [[CrossRef](#)]
53. Pringle, M.J.; Schmidt, M.; Muir, J.S. Geostatistical interpolation of SLC-off Landsat ETM+ images. *ISPRS J. Photogramm. Remote Sens.* **2009**, *64*, 654–664. [[CrossRef](#)]
54. Zhang, C.; Li, W.; Travis, D. Gaps-fill of SLC-off Landsat ETM+ satellite image using a geostatistical approach. *Int. J. Remote Sens.* **2007**, *28*, 5103–5122. [[CrossRef](#)]
55. Liu, C.-Y.; Chen, C.; Chang, C.T.; Shih, L.M. Single-hidden-layer feed-forward quantum neural network based on grover learning. *Neural Netw.* **2013**, *45*, 144–150. [[CrossRef](#)] [[PubMed](#)]
56. García, S.R.; Romo, M.P.; Mayoral, J.M. Estimation of peak ground accelerations for Mexican subduction zone earthquakes using neural networks. *Geofis. Int.* **2007**, *46*, 51–62.
57. Mas, J.F.; Flores, J.J. The application of artificial neural networks to the analysis of remotely sensed data. *Int. J. Remote Sens.* **2007**, *29*, 617–663. [[CrossRef](#)]
58. Mofidi, A.; Soltanzadeh, I.; Yousefi, Y.; Zarrin, A.; Soltani, M.; Masoompour Samakosh, J.; Azizi, G.; Miller, S.T.K. Modeling the exceptional South Foehn Event (GARMII) over the alborz mountains during the extreme forest fire of December 2005. *Nat. Hazard.* **2014**, *75*, 2489–2518. [[CrossRef](#)]
59. Özelkan, E.; Örmeci, C. Risk assessment of forest fires by using satellite data with remote sensing techniques. In *Proceedings of the 28th Remote Sensing for a Changing Europe*, Istanbul, Turkey, 2–5 June 2008.
60. Jolly, W.M. Sensitivity of a surface fire spread model and associated fire behaviour fuel models to changes in live fuel moisture. *Int. J. Wildland Fire* **2007**, *16*, 503–509. [[CrossRef](#)]
61. Chuvieco, E.; Cocero, D.; Riaño, D.; Martín, P.; Martínez-Vega, J.; de la Riva, J.; Pérez, F. Combining NDVI and surface temperature for the estimation of live fuel moisture content in forest fire danger rating. *Remote Sens. Environ.* **2004**, *92*, 322–331. [[CrossRef](#)]
62. Molavi-Arabshahi, M.; Arpe, K.; Leroy, S.A.G. Precipitation and temperature of the Southwest Caspian Sea region during the last 55 years: Their trends and teleconnections with large-scale atmospheric phenomena. *Int. J. Climatol.* **2016**, *36*, 2156–2172. [[CrossRef](#)]
63. Lopes, S.; Viegas, D.X.; de Lemos, L.; Viegas, M.T. Rainfall effects on fine forest fuels moisture content. In *Advances in Forest Fire Research*; Imprensa da Universidade de Coimbra: Coimbra, Portugal, 2014; p. 427.
64. Van Wagner, C.; Forest, P. *Development and Structure of the Canadian Forest Fireweather Index System*; Canada Forest Service: Ottawa, ON, Canada, 1987.
65. Tucker, C.J. Remote sensing of leaf water content in the near infrared. *Remote Sens. Environ.* **1980**, *10*, 23–32. [[CrossRef](#)]

66. Gates, D.M.; Keegan, H.J.; Schleiter, J.C.; Weidner, V.R. Spectral properties of plants. *Appl. Opt.* **1965**, *4*, 11–20. [[CrossRef](#)]
67. Bowyer, P.; Danson, F.M. Sensitivity of spectral reflectance to variation in live fuel moisture content at leaf and canopy level. *Remote Sens. Environ.* **2004**, *92*, 297–308. [[CrossRef](#)]
68. Leghari, S.K.; Zaidi, M.A.; Sarangzai, A.M. Seasonal variation in leaf relative water, dry matter and live fine fuel moisture contents in some common plant species of Quetta, Balochistan. *FUUAST J. Biol.* **2013**, *3*, 73–76.
69. Tanentzap, F.M.; Stempel, A.; Ryser, P. Reliability of leaf relative water content (RWC) measurements after storage: Consequences for in situ measurements. *Botany* **2015**, *93*, 535–541. [[CrossRef](#)]
70. Mataix-Solera, J.; Cerdà, A.; Arcenegui, V.; Jordán, A.; Zavala, L.M. Fire effects on soil aggregation: A review. *Earth Sci. Rev.* **2011**, *109*, 44–60. [[CrossRef](#)]
71. Yang, X.; Guo, X.; Fitzsimmons, M. Assessing light to moderate grazing effects on grassland production using satellite imagery. *Int. J. Remote Sens.* **2012**, *33*, 5087–5104. [[CrossRef](#)]
72. Keane, E.R. Fuel moisture. In *Wildland Fuel Fundamentals and Applications*; Springer International Publishing: Cham, Germany, 2015; pp. 71–82.
73. Finney, M.A. *Farsite: Fire Area Simulator: Model Development and Evaluation*; US Department of Agriculture, Forest Service, Rocky Mountain Research Station Ogden: Fort Collins, CO, USA, 2004.
74. Nolan, R.H.; Resco de Dios, V.; Boer, M.M.; Caccamo, G.; Goulden, M.L.; Bradstock, R.A. Predicting dead fine fuel moisture at regional scales using vapour pressure deficit from MODIS and gridded weather data. *Remote Sens. Environ.* **2016**, *174*, 100–108. [[CrossRef](#)]
75. Hardwick, S.R.; Toumi, R.; Pfeifer, M.; Turner, E.C.; Nilus, R.; Ewers, R.M. The relationship between leaf area index and microclimate in tropical forest and oil palm plantation: Forest disturbance drives changes in microclimate. *Agric. For. Meteorol.* **2015**, *201*, 187–195. [[CrossRef](#)]
76. Punalekar, S.; Verhoef, A.; Tatarenko, I.V.; van der Tol, C.; Macdonald, D.M.; Marchant, B.; Gerard, F.; White, K.; Gowing, D. Characterization of a highly biodiverse floodplain meadow using hyperspectral remote sensing within a plant functional trait framework. *Remote Sens.* **2016**, *8*, 112. [[CrossRef](#)]
77. Ray, D.; Nepstad, D.; Brando, P. Predicting moisture dynamics of fine understory fuels in a moist tropical rainforest system: Results of a pilot study undertaken to identify proxy variables useful for rating fire danger. *New Phytol.* **2010**, *187*, 720–732. [[CrossRef](#)] [[PubMed](#)]
78. Chen, J.; Saunders, S.C.; Crow, T.R.; Naiman, R.J.; Brosofske, K.D.; Mroz, G.D.; Brookshire, B.L.; Franklin, J.F. Microclimate in forest ecosystem and landscape ecology: Variations in local climate can be used to monitor and compare the effects of different management regimes. *BioScience* **1999**, *49*, 288–297. [[CrossRef](#)]
79. Merzouki, A.; Leblon, B. Mapping fuel moisture codes using MODIS images and the getis statistic over western canada grasslands. *Int. J. Remote Sens.* **2011**, *32*, 1619–1634. [[CrossRef](#)]
80. Wang, L.; Hunt, E.R., Jr.; Qu, J.J.; Hao, X.; Daughtry, C.S.T. Remote sensing of fuel moisture content from ratios of narrow-band vegetation water and dry-matter indices. *Remote Sens. Environ.* **2013**, *129*, 103–110. [[CrossRef](#)]
81. Trombetti, M.; Riaño, D.; Rubio, M.A.; Cheng, Y.B.; Ustin, S.L. Multi-temporal vegetation canopy water content retrieval and interpretation using artificial neural networks for the continental USA. *Remote Sens. Environ.* **2008**, *112*, 203–215. [[CrossRef](#)]
82. Yebra, M.; Dennison, P.E.; Chuvieco, E.; Riaño, D.; Zylstra, P.; Hunt, E.R., Jr.; Danson, F.M.; Qi, Y.; Jurdao, S. A global review of remote sensing of live fuel moisture content for fire danger assessment: Moving towards operational products. *Remote Sens. Environ.* **2013**, *136*, 455–468. [[CrossRef](#)]
83. Chuvieco, E.; Riano, D.; Aguado, I.; Cocero, D. Estimation of fuel moisture content from multitemporal analysis of landsat thematic mapper reflectance data: Applications in fire danger assessment. *Int. J. Remote Sens.* **2002**, *23*, 2145–2162. [[CrossRef](#)]
84. Riano, D.; Vaughan, P.; Chuvieco, E.; Zarco-Tejada, P.J.; Ustin, S.L. Estimation of fuel moisture content by inversion of radiative transfer models to simulate equivalent water thickness and dry matter content: Analysis at leaf and canopy level. *IEEE Trans. Geosci. Remote Sens.* **2005**, *43*, 819–826. [[CrossRef](#)]
85. Jurdao, S.; Yebra, M.; Guerschman, J.P.; Chuvieco, E. Regional estimation of woodland moisture content by inverting radiative transfer models. *Remote Sens. Environ.* **2013**, *132*, 59–70. [[CrossRef](#)]
86. Mendiguren, G.; Pilar Martín, M.; Nieto, H.; Pacheco-Labrador, J.; Jurdao, S. Seasonal variation in grass water content estimated from proximal sensing and modis time series in a mediterranean fluxnet site. *Biogeosciences* **2015**, *12*, 5523–5535. [[CrossRef](#)]

87. Liang, S.; Strahler, A.H.; Jin, X.; Zhu, Q. Comparisons of radiative transfer models of vegetation canopies and laboratory measurements. *Remote Sens. Environ.* **1997**, *61*, 129–138. [[CrossRef](#)]
88. Widlowski, J.-L.; Mio, C.; Disney, M.; Adams, J.; Andredakis, I.; Atzberger, C.; Brennan, J.; Busetto, L.; Chelle, M.; Ceccherini, G.; et al. The fourth phase of the radiative transfer model intercomparison (RAMI) exercise: Actual canopy scenarios and conformity testing. *Remote Sens. Environ.* **2015**, *169*, 418–437. [[CrossRef](#)]
89. Atzberger, C.; Darvishzadeh, R.; Immitzer, M.; Schlerf, M.; Skidmore, A.; le Maire, G. Comparative analysis of different retrieval methods for mapping grassland leaf area index using airborne imaging spectroscopy. *Int. J. Appl. Earth Obs. Geoinf.* **2015**, *43*, 19–31. [[CrossRef](#)]
90. Yilmaz, M.T.; Hunt, E.R., Jr.; Jackson, T.J. Remote sensing of vegetation water content from equivalent water thickness using satellite imagery. *Remote Sens. Environ.* **2008**, *112*, 2514–2522. [[CrossRef](#)]
91. Saito, K.; Ogawa, S.; Aihara, M.; Otowa, K. Estimates of Lai for forest management in Okutama. In Proceedings of the 22nd Asian Conference on Remote Sensing, Singapore, 5–9 November 2001.
92. Su, B.; Wang, M.S.L. *Help for Sebs 4 ILWIS, Water Resources (SEBS)*; 52° North ITC: Enschede, The Netherlands, 2010.
93. Liang, S. *Quantitative Remote Sensing of Land Surfaces*; Wiley-Interscience: Hoboken, NJ, USA, 2005.
94. Liang, S.; Shuey, C.J.; Russ, A.L.; Fang, H.; Chen, M.; Walthall, C.L.; Daughtry, C.S.T.; Hunt, R., Jr. Narrowband to broadband conversions of land surface albedo: II. Validation. *Remote Sens. Environ.* **2003**, *84*, 25–41. [[CrossRef](#)]
95. Chander, G.; Markham, B. Revised Landsat-5 TM radiometric calibration procedures and postcalibration dynamic ranges. *IEEE Trans. Geosci. Remote Sens.* **2003**, *41*, 2674–2677. [[CrossRef](#)]
96. Tursilowati, L.; Djundjuran, J.D. Use of remote sensing and GIS to compute temperature humidity index as human comfort indicator relate with Land Use-Land Cover change (LULC) in Surabaya. In Proceedings of the 73rd International Symposium on Sustainable Humanosphere, Bandung, Indonesia, 22–25 July 2007; pp. 160–166.
97. Adab, H.; Kanniah, K.; Solaimani, K.; Tan, K.P. Estimating atmospheric humidity using MODIS cloud-free data in a temperate humid region. In Proceedings of the 2013 IEEE International Geoscience and Remote Sensing, Melbourne, Australia, 21–26 July 2013.
98. Yoder, B.J.; Waring, R.H. The normalized difference vegetation index of small douglas-fir canopies with varying chlorophyll concentrations. *Remote Sens. Environ.* **1994**, *49*, 81–91. [[CrossRef](#)]



© 2016 by the authors; licensee MDPI, Basel, Switzerland. This article is an open access article distributed under the terms and conditions of the Creative Commons Attribution (CC-BY) license (<http://creativecommons.org/licenses/by/4.0/>).